Volume 2, Number 1, 2009. pp. 1-46

Jordan Journal of Physics

REVIEW ARTICLE

Magneto-Optical and Magneto-Dielectric Anisotropy Effects in Magnetic Fluids

N.A. Yusuf and **I. O. Abu-Aljarayesh**

Department of Physics, Yarmouk University, Irbid, Jordan.

Received on: 21/8/2008; Accepted on: 10/3/2009

Abstract: An overview of the magneto-optical and magneto-dielectric effects in magnetic fluids is presented encompassing experimental results and different phenomenological models used to explain these effects. The role of the different parameters on these effects, are discussed. It is suggested that the field induced-mechanical anisotropy produced by agglomeration and chain formation in magnetic fluids is the main cause for these magneto-optical and magneto-dielectric effects in magnetic fluids.

Keywords: Magneto-optics, Magnetic fluids, Faraday rotation, Faraday ellipticity, Transmission, Optical anisotropy, Birefringence, Dichroism, Degree of polarization, Polarization effects, Magneto-dielectric effects, Dielectric anisotropy, Chain formation.

Introduction

Under the application of external magnetic fields, magnetic fluids, MF's, exhibit a range of magneto-effects such as magneto-optical and magneto-dielectric effects.

Magneto-optical effects in magnetic fluids, have been investigated by many researchers using different experimental techniques as well as different theoretical approaches because of their promising potential for technological and industrial applications as well as their academic importance [1-24]

The work on magneto-optical effects has started as early as the middle of nineteenth century. Scholten has reviewed the early work in magneto-optical effects in colloids and showed the importance of these studies in obtaining information about the magnetic particles and their spatial relations [25].

The magneto-optical effects to be addressed in this review are: Birefringence, Dichroism, Faraday rotation, Faraday ellipticity, Degree of polarization and the transmission of light; as well as magneto-dielectric anisotropy effect.

The induced magneto-optical and magneto-dielectric effects in magnetic fluids are generally believed to be due to either field-induced magnetic or mechanical anisotropies in the fluid.

This review is organized as follows: In section one the texture in MF's is addressed. In section two the magneto-optical effects in MF's and their dependence on the various parameters (magnetic field, concentration of magnetic particles, wavelength of the incident electromagnetic waves and temperature) are presented. In section three the magneto-dielectric anisotropy effect in MF's is presented. In the last section, numerical calculations of the magneto-optical and magneto-dielectric effects are presented.

1- Texture in Magnetic Fluids

Under the application of external magnetic fields, magnetic fluids become textured. This texture could be a magnetic texture due to the alignment of the permanent dipole moments in the field direction, or it could be

Corresponding Author: N. A. Yusuf. **Email**: nihadyusuf@yu.edu.jo

mechanical one due to the agglomeration of particles and chain formation in fluids.

Colloidal suspensions of ferromagnetic particles in magnetically passive liquid carriers have been found in different states of aggregation depending upon temperature, concentration of the magnetic particles and external magnetic fields. These systems have been observed to form long chains as well as large compact clusters. Aggregation and chain formation are assumed to be the main cause for the appearance of most magneto-optical effects in magnetic fluids [5-24].

Theoretical studies of chain formation in magnetic fluids based on particle-particle interaction were first carried out by De Gennes and Pincus [26]. The main findings of this study can be summarized for the low concentration of magnetic particles in magnetic fluids as follows: for large external magnetic fields the particles tend to form long chains along the field direction. In the absence of external field short chains still exist and behave like rods but randomly oriented. Moreover as a chain length becomes more than 4 D (D is the diameter of the particle) the lowest energy conformation is a ring, leading to magnetic flux closure, thus the longer chains either break into shorter chains or close on it self. Elfimova [33] has attempted to establish a theoretical model for the fractal-like clusters induced in magnetic fluids and concluded that an analytical result is rather difficult to obtain.

For chain formation to be established in a magnetic fluid, the magnetic particles must relax through the Brownian relaxation mechanism, *i.e.,* they should rotate physically in the field direction with their magnetic moments fixed in their easy axis direction with a relaxation time τ_B [37].

Another competing mechanism is the N$e'el$ relaxation mechanism through which the magnetic moments of the particles rotate against the anisotropy field and align in the field direction in a time τ_N [37].

The relaxation mechanism with the shortest relaxation time will dominate the relaxation process of the particles. Particles, relaxing via the N$e'el$ relaxation mechanism, do not contribute to chain formation or to the mechanical anisotropy in the sample.

When the sample is in the frozen state, its viscosity is very high and the Brownian relaxation time is very large, consequently, the particles relax via the N$e'el$ relaxation mechanism. However, when the sample is in the liquid state both relaxation mechanisms are available for the particles, and some particles relax via the Brownian relaxation mechanism while the others relax via the N$e'el$ relaxation mechanism depending on the volume of the particles and the temperature of the sample. As will be shown when discussing the temperature dependence of magneto-optical effects the onset of the Brownian relaxation occurs when the two relaxation times become equal (starting from the frozen state of the sample). This equality occurs for a given volume of the particles known as the Shliomis volume V_S. The Shliomis volume depends in a rather complex manner on temperature, viscosity, applied magnetic field, concentration and the size and shape of the particles. Particles with volumes $V \geq V_S$ relax via the Brownian relaxation mechanism and thus contribute to the chain formation in the sample. Although the onset of the physical orientation of the particles in the field direction, and the chain formation is determined by the competition between those two relaxation mechanisms, the degree of orientation of the particles, and chain length or number of chains in the sample depend on other parameters. Although the temperature and the applied field play direct and indirect roles in the relaxation times τ_N and τ_B, they play two competing roles once orientation of particles and chain formation have started. The field plays an orienting role while the temperature plays a randomizing role due to thermal agitation. At low temperatures the orienting role of the field is dominant, but at higher temperatures the randomizing role of temperature becomes dominant.

Two more parameters are crucial in the chain formation in the samples. The first is the interaction of the magnetic moments with the field, *i.e.,* the Zeeman interaction which favors energy-wise more chains and longer chains, and the chain- chain interaction which energy-wise favors less number of chains, shorter chains and larger separation between chains. It is important to mention that this chain-chain interaction becomes much stronger once the concentration of the sample is increased and may lead to the curling or even the closure of some chains. It is also important to mention that most experimental investigation, based on optical observation, on the chain formation in magnetic fluids are usually carried out on samples in the low concentration regime where chain-chain interaction is weak [14,26].

It is the interplay of all these parameters that determines the “optimum conditions” for chain formation in magnetic fluids and, consequently all other magneto-optical and magneto-dielectric effects.

It is the complex nature of these parameters and even the more complex nature of their interplay, we believe, that rendered the development of a complete analytical theory for chain formation in magnetic fluids a formidable task. Therefore one has to rely on the available experimental and of Monte-Carlo simulation results. In most of the experimental work on chain formation in magnetic fluids, the samples are usually contained in a transparent cell placed in a magnetic field. The dimension of the cell in the field direction plays an important role on the length and number of chains formed in the sample. For low dimension cells (thin film case), a spatial limitation on the chain length is imposed resulting in a “premature saturation” in the length, well before the optimum conditions determined by the above discussed competing parameters is reached, and the faster formation of new chains.

Some experimental observations of chain formation have been indirect; Haas and Adams [5] concluded that chains had formed from the diffraction pattern, characteristic of a grating, found when light is passed through a sample of magnetite-based ferrofluids perpendicular to the applied field. Popplewell *et al* [6] have investigated the chain formation in magnetic fluid composite thin films and have shown both experimentally and by Monte Carlo simulation that extensive chain formation occurs in relatively weak magnetic fields. They have also shown that the chain length varies with the concentration according to the empirical formula $l \alpha C^{312.}$

Detailed experimental study on the field-induced agglomeration in thin films of water-based magnetic fluids has been reported by Jones and Niedoba [27]. An experimental investigation of the chain formation in magnetic fluids was also carried out by Yusuf [28]. Recently Fang *et al*. [31] carried out an experimental study on the magnetic-field-induced chain-like assembly structures in magnetic fluids. In their work they have observed extensive chain formation under the application of magnetic fields. Fang et al. suggested that the structure takes place in a two stage process, aggregation among particles to form chains, and aggregation among the chains to form linear clusters, which are also active in forming the observed aligned structures. Furthermore, they have also suggested that the chain length is some times determined by the physical dimensions of the sample [31].

Another recent study on chain-like aggregates in magnetic fluids was undertaken by Pshenichnikova, and Fedorenkob [30] using cross-fields measurements. The bias field is a direct field while the measuring field is an alternating field. Pshenichnikova, and Fedorenkob concluded that chain formation was absent in highly concentrated samples and that short chains existed in diluted samples. They have attributed this to the fact that, in a concentrated sample, the closed-ring structure is more stable than long chains. They have also suggested that shielding of the magneto- dipole interactions reduces the possibility of chain formation. Diluting the sample reduces the role of shielding and breaks the balance between the attractive interactions and the steric-repulsive interaction, thus increases the chances of chain formation.

In their work, Jones and Niedoba [27] had a drop of undiluted fluid sandwiched between two parallel glass cover slips and placed normal to the optic axis of a microscope. The magnetic field was applied parallel to the axis of the microscope, i.e. perpendicular to the plane of the thin film sample. In this experimental arrangement Jones and Niedoba observed the number of chains per unit volume, n, and found it to increase rapidly with the applied field. The experimental set up used by Jones and Niedoba put sever limitation on the length of formed chains and lead to premature saturation in the chain lengths as was suggested by Fang *et al* [31].

In his work, Yusuf [28] has avoided this premature saturation in the chain length by increasing the sample length in the field direction. The field and concentration dependence of chain formation in Fe_30_4 particle magnetic fluid was investigated. The saturation magnetizations of the samples used are 5, 10, 15, 20 and 25 kA/m (saturation magnetization of bulk Fe_3O_4 is 485 kA/m). Thus these samples are diluted samples. Magnetic fields up to 71.6 kA/m are used in this work. Fig.1 shows the diffraction pattern obtained when light was incident normal to the field and the plane of the fluid. The diffraction pattern observed is similar to the pattern produced by a diffraction grating and thus provided indirect evidence on the chain formation in the fluid.

The experimental set-up for observing the chain formation in the magnetic fluid is shown in Fig.2.

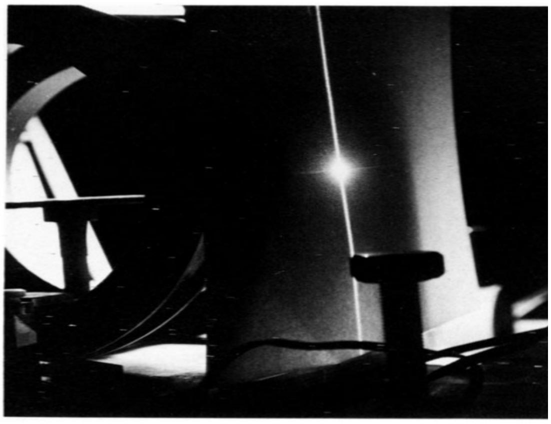

FIG. 1. The diffraction pattern observed by shining a laser beam normal to the field and plane of the fluid.

For viewing the chains the magnetic field is applied parallel to the plane of the fluid and perpendicular to the optical axis of the microscope, and for viewing the cross-section of the chains the field is applied perpendicular to the plane of the fluid and parallel to the optical axis of the microscope.

In Fig.3, An optical micrograph for 15 kA/m saturation magnetization magnetic fluid samples under 33.4 kA/m magnetic field showing chain formation is presented, and in Fig.4, an optical micrograph for the same sample showing the cross-section of the chains is presented.

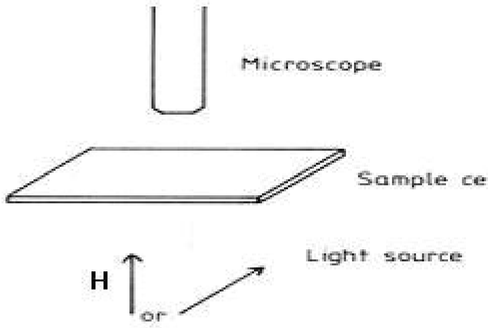

FIG. 2. Viewing arrangement of the chains formed in magnetic fluids

The chain length in magnetic fluid with saturation magnetization of 15 kA/m sample as a function of applied magnetic field is shown in Fig.5.

The results in the figure show that the chain length increases sharply at low fields reaching ≈ 0.5 mm at relatively weak fields. A gradual increase in the chain length is observed for intermediate fields and at high fields a tendency towards saturation is observed.

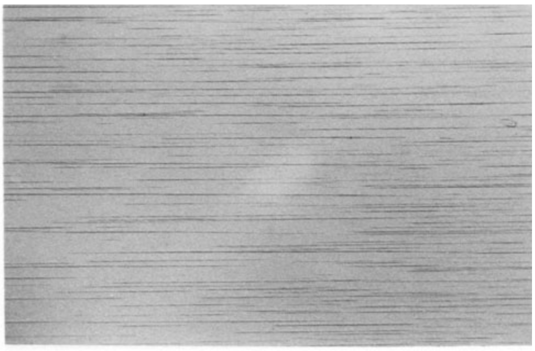

FIG. 3. An optical micrograph for 15 kA/m saturation magnetization magnetic fluid under 33.4 kA/m magnetic field parallel to the plane of the fluid.

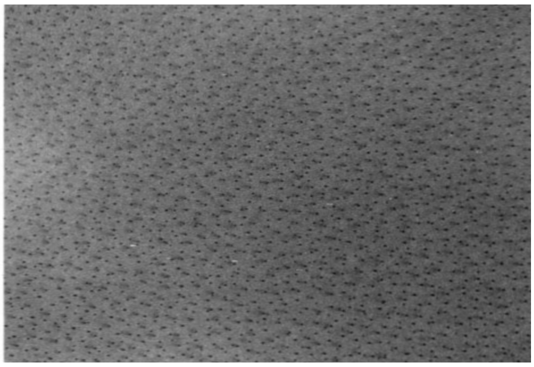

FIG. 4. An optical micrograph obtained by viewing the sample parallel to an applied magnetic field H = 15..9 kA/m

In Fig.6 the chain length under the application of an intermediate magnetic field (33.4 kA/m) is shown as a function of concentration (low concentration regime) of the magnetic fluid.

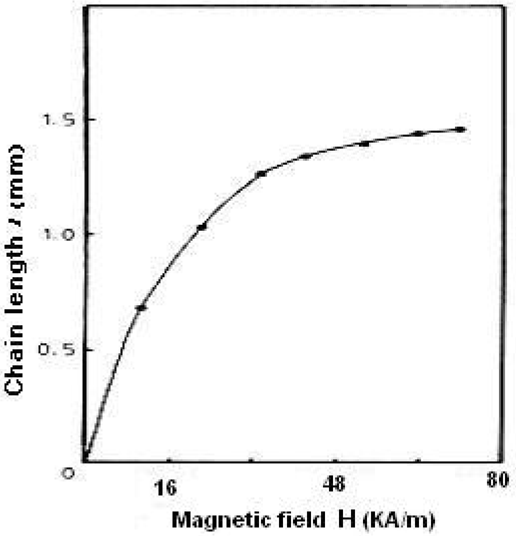

FIG. 5. The average chain length in a 15 kA/m saturation magnetization sample versus applied magnetic field

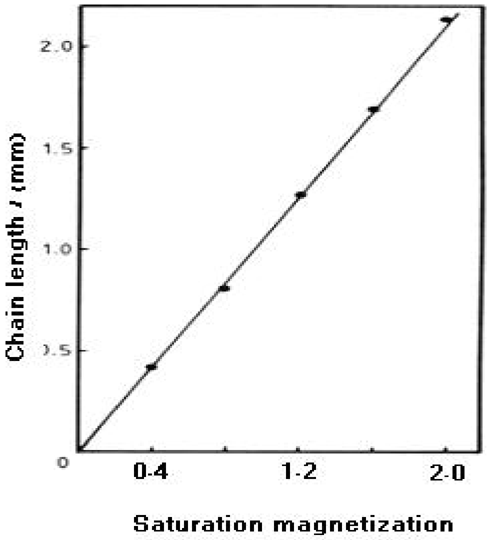

FIG. 6. The average chain length at H = 33.4 kA/m versus the saturation magnetization of the fluid.

The results show that the chain length at intermediate field, i.e., before saturation, the chains length, is linear with saturation magnetization. It is worth mentioning that for thin samples, the chain length approaches the thickness of the sample at very low fields and saturates prematurely. Consequently, the chain length is not expected to increase any further with the field but rather an increase in the number of chains is observed. The role of texture and chain formation on magneto-optical effects will be discussed in the following sections. The different relationships between chain length and concentration obtained by different workers may be attributed to the dependence of the chain length on other parameters such as the field, temperature and spatial limitations imposed by the cells used in containing the sample under investigation[32, 60, 61].

2- Magneto-Optical Effects in Magnetic Fluids

In this section the magneto-optical effects including transmission, Faraday rotation, Faraday ellipticity, birefringence and dichroism are presented. The role of texture and the various parameters on these magneto-optical effects is discussed.

2.1- Magneto-Optical Effects and Texture in the Fluid

2.1.1- Linear Birefringence and Dichroism

Birefringence, Δn, is defined as the difference between two indices of refraction one is for an electromagnetic wave linearly polarized in a given direction parallel to magnetic field direction, ($n_{\|}$), and the other for an electromagnetic wave linearly polarized in direction perpendicular to the magnetic field direction, ($n_{\perp}$). Dichroism, ΔA however is defined as the difference in selective absorption between these two orthogonal states.

Birefringence and dichroism have been measured by many investigators using different techniques [21, 56]

Recently Kooij *et al.* [57] has measured dichroism and birefringence in magnetite magnetic fluids using transmission ellipsometry. Using this technique they have investigated the spectral dependence of birefringence and dichroism and got good agreement with previous studies [69].

Here, we present some of the experimental results relating birefringence to the texture in magnetic fluids.

Davies and Llewellen [11] have observed birefringence in a thin film of magnetic fluid sandwiched between thin slide covers when it was in the liquid state. However, when the magnetic fluid was dried under zero fields, birefringence was not observed and by adding a drop of liquid carrier to the dried sample, birefringence was observed once again.

Bacri *et al.* [13] has implanted Fe_3O_4 magnetic particles in a gel matrix and applied a magnetic field but they observed no birefringence.

Yusuf and co-workers [19] have studied birefringence in the temperature range 100-325 K. Two experimental procedures were followed, the first by cooling the sample to the low temperature with no field applied. Then by applying an external magnetic field, the birefringence was measured. The results in Fig.7 show that birefringence is absent at low temperatures and continues to be absent till a specific temperature is reached then a weak birefringence is observed. At this temperature the fluid is in a slurry state. By further increase in the temperature a steep increase in the birefringence is observed (the fluid has reached its melting temperature) reaching a maximum value. Beyond this maximum an increase in temperature results in the reduction of birefringence.

The second approach is done by applying a magnetic field on the sample starting from high temperature and then cooling the sample while the field is applied. The results also (Fig.7) show that the birefringence increases by decreasing the temperature reaching a maximum value. Further decrease of temperature does not change the value of birefringence.

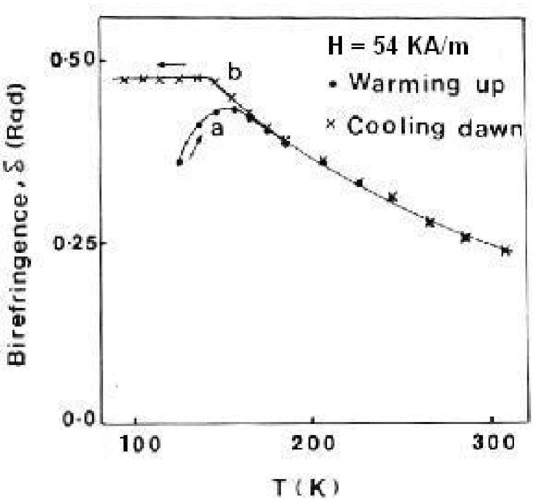

FIG. 7. Birefringence versus temperature, a) warming up and b) cooling down.

Discussion of this behavior is presented in the section devoted to the temperature dependence of birefringence and dichroism.

Drying the sample, implanting the magnetic particles in a gel matrix or freezing the magnetic fluid sample, have the same common effect of preventing the physical motion of the particles and thus prohibiting agglomeration and chain formation in the sample. Therefore, the belief that the magneto optical anisotropy, *i.*e, birefringence and dichroism, in magnetic fluids are due to the field-induced mechanical anisotropy of the sample is well established.

2.1.2- Circular Birefringence and Transmission of Light

Faraday rotation is defined as the rotation of the direction of polarization of a plane polarized electromagnetic wave around its propagation direction. This is usually explained in terms of the difference in the indices of the two circularly polarized components, R- state and L -state. Faraday ellipticity, however, is a measure of the difference between the amplitudes of these two circularly polarized states.

Faraday rotation, Faraday ellipticity and the transmission of light through a magnetic fluid were investigated by some workers in the field [54-56, 58, 29].

Taketomi [54] studied the absorption of light in thin films of magnetic fluids. Taketomi used two different concentrations and two different thicknesses. It was shown that the absorption increases with concentration and thickness.

Davies *et al.* [55] has studied the transmission of microwaves through magnetic fluids and showed that the transmission follows a Langevin- type behavior with the field similar to the magnetization of the fluid.

Davies and Llewellen [56] have measured Faraday rotation in highly diluted samples of Fe_3O_4 and Co particle magnetic fluid. Again their results suggested a Langevin-type behavior similar to the magnetization of the samples. From their results they concluded that Faraday rotation is governed by the magnetization of the samples.

Rousan *et al.* [58] has investigated the dependence of the transmission of light on the applied field and the concentration of the sample. In this investigation the propagation of light is parallel to the applied field. The transmission coefficient R defined as the ratio of increase in the intensity of the transmitted light at a magnetic field H to the intensity of the transmitted light at zero applied fields was measured for samples with different concentration, and for samples of the same concentration but with different surfactant contents. Furthermore, the coefficient R was measured for the same sample but at two different thicknesses. Their results show that R follows a Langevin-type behavior i.e., increasing almost linearly with the field at low fields then gradually at intermediate fields tending to saturate at high fields. However Swapna *et al.* [29] in their recent study on the transmission of light have used a different configuration. In their configuration the propagation of light is normal to the applied magnetic field. Swapna *et al.* [26] results show that the transmission of light decreases with the applied field steeply at low fields and then gradually at intermediate fields reaching almost a constant value at high fields. It is important to mention that the results of Swapna *et al.* [29] and those of Rousan *et al.* [59] are almost mirror image of each other about the field axis. Both of these two groups attributed the change in the transmission to the agglomeration and chain formation in the magnetic fluid. Rousan *et al.* suggested that due to the chain formation under the application of magnetic fields, the scattering cross-sectional area of the particles decreases and the sample is arranged mechanically allowing for the "channeling" of light in a direction parallel to the applied field. Therefore, the transmission increases with the field. Using similar ideas but increasing the scattering cross sections and partial "blocking" instead of "channeling" the decrease in the transmission observed by Swapna *et al.* [29] may be explained. In their work, Rousan *et al* [58] has measured the transmission of light for the same sample at two different thicknesses 0.2 and 1 mm. The results in Fig.8 show that the transmission coefficient R for the thick sample is much higher than that for the thin sample. Furthermore, they show that R reaches saturation in the thin sample while it is still increasing appreciably for the thick sample.

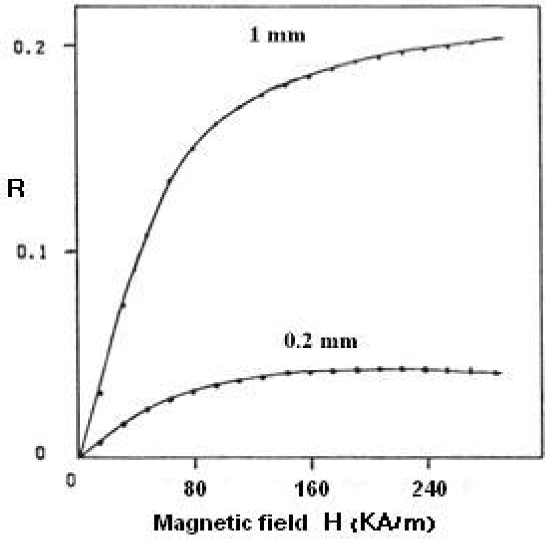

FIG. 8. Transmission coefficient versus applied field at two different thicknesses.

This behavior is attributed to the "premature" saturation of the chains in the thin samples.

The same workers have also measured the transmission coefficient in three samples with the same particle concentration, same liquid carrier but with slightly different surfactant contents.

Their results presented in Fig.9 show that the higher the surfactant content in the sample is, the lower the transmission coefficient is and the faster it approaches saturation.

These results may be explained as follows: decreasing the surfactant content of the sample breaks the balance between the attractive interactions and the repulsive interaction in favor of the attractive ones. Thus the possibility of chain formation is increased [30] and consequently, the transmission is increased.

The concentration and field dependence of Faraday rotation was thoroughly investigated by Yusuf and co-workers [58-61] by studying samples with saturation magnetization (6-100 kA/m).

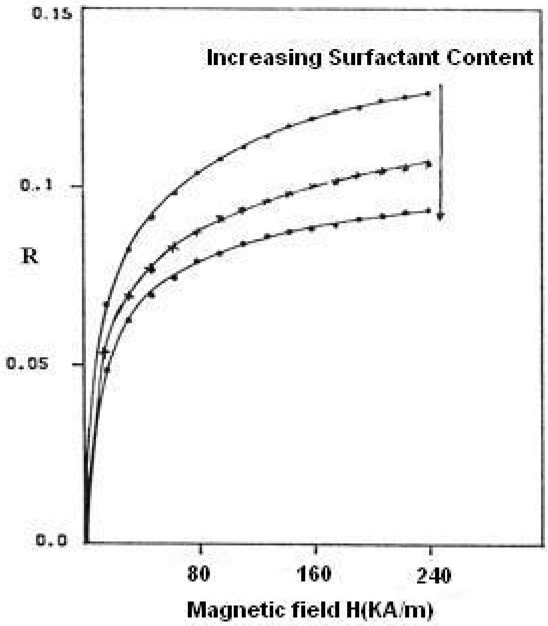

FIG. 9. Transmission coefficient (R) versus field for different surfactant contents.

Fig.10 shows Faraday rotation, β for samples with saturation magnetization (6-25 kA/m) and thickness of 1 mm. The results show that β follows a Langevin-type behavior that is increasing sharply with the field at low fields and tends to saturate at high fields similar to the magnetization of the samples. Furthermore the results also show that β increases with the concentration of the sample and tends to saturate at higher fields for higher concentrations.

Faraday rotation β was measured for two identical samples but with two different thicknesses. The results are presented in Fig.11.

The results show that Faraday rotation in the thick sample is larger than that in the thin sample and surprisingly it saturates at fields for the thicker sample higher than those needed to saturate it for the thinner sample.

Faraday rotation β was also measured for samples of the same concentration but with slightly different surfactant contents. The results are shown in Fig.12.

The results show that Faraday rotation increases with decreasing surfactant contents and saturates at higher fields when the surfactant content is decreased as was previously explained.

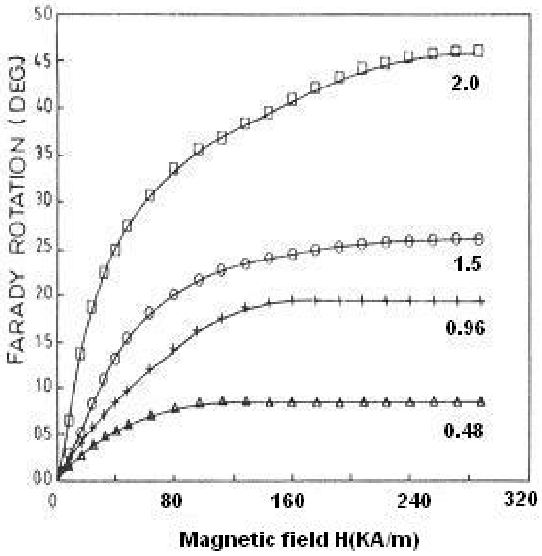

FIG. 10. Faraday rotation versus field for different saturation magnetization.

If Faraday rotation is only governed by the magnetization of the sample then the saturation will take place at practically the same applied field for the same sample regardless of the thickness of the sample. The difference in the saturation field is attributed to the chain formation in the sample. As was mentioned above, chain formation may prematurely saturate in thin samples due to the physical limitation imposed on the sample.

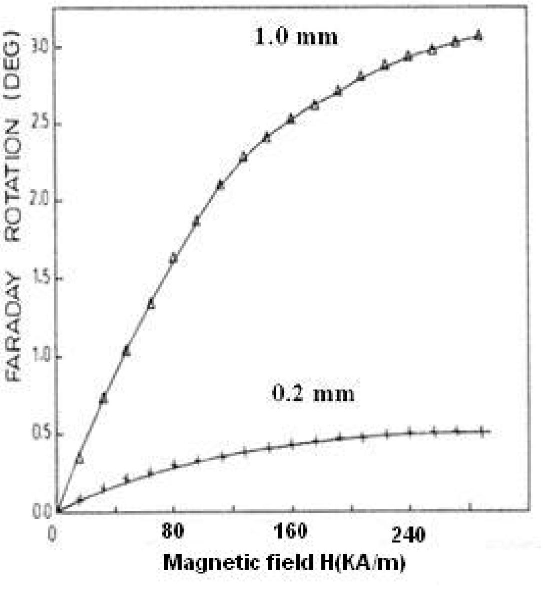

FIG. 11. Faraday rotation versus applied field at two different thicknesses.

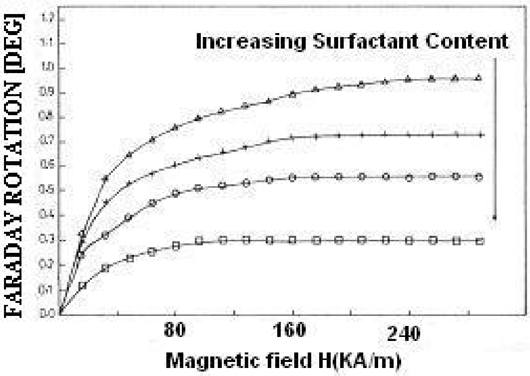

FIG. 12. Faraday rotation versus field for different surfactant contents.

As will be shown in the section on the temperature dependence of magneto-optical effects, a weak Faraday rotation is still observed in the frozen magnetic fluid when chain formation is physically prohibited. It is therefore believed that both magnetization and chain formation contribute to the Faraday rotation in magnetic fluids; and here we attempt to separate these two contributions.

Usually, for a homogeneous colloidal suspension of single domain fine ferromagnetic particles, the Faraday rotation is given by:

$$\beta_M(H) = C\frac{M(H)}{M_S} \tag{1}$$

where $\beta_M(H)$ is the Faraday rotation at magnetic field H, $M(H)$ is the magnetization of the sample at magnetic field H, M_S is the saturation magnetization of the sample and C is a constant.

In order to explain the results presented in Figs. (8, 9, 11-12), Yusuf and co-workers [60], introduced a new term to the Faraday rotation, β by invoking the Verdet law. This term which is due to the chain formation is given by:

$$\beta_C(H) = VHl(H) \tag{2}$$

where $\beta_C(H)$ is the Faraday rotation due to the chain formation, H is the 'local' field, $l(H)$ is the chain length at field H and V is the Verdet constant.

The total Faraday rotation β is then given by:

$$\beta(H) = C\frac{M(H)}{M_S} + VHl(H) \tag{3}$$

Since both the magnetization of the sample and the chain formation for weakly interacting system follow a Langevin- type behavior, Faraday rotation β is assumed to follow a Langevin- type behavior expressed as:

$$\beta(H) = \beta_S L(aH) \tag{4}$$

where β_S is the saturation Faraday rotation, and a is a parameter that is saturation magnetization dependent.

The values of β_S are graphically obtained by plotting the inverse of β against the inverse of the magnetic field H. By plotting the reduced Faraday rotation (β/β_S) versus magnetic field, Yusuf and co-workers [60] showed that for a given reduced Faraday rotation the magnetic field is higher for higher saturation magnetization which implies that the parameter a is lower for higher saturation magnetization. Furthermore, they have obtained the parameter, a from the linear part of the reduced Faraday rotation curves and showed that it is inversely proportional to the saturation magnetization.

In the experimental work of Yusuf and co-workers, Faraday rotation was measured using electromagnetic waves of wavelength (λ = 600 nm) which is at least three orders of magnitude less than the chain length. Consequently, the local field felt by the electromagnetic waves is practically constant and thus the contribution to Faraday rotation due to chain formation particularly at high fields is constant. Accordingly, Faraday rotation β is written as:

$$\beta = C\frac{M(H)}{M_S} + C' \tag{5}$$

where C' is the maximum contribution of the chain formation to the Faraday rotation. Plotting β versus ($M(H)/M_S$), C' is obtained for different samples with different saturation magnetization and it is found to be linear with saturation magnetization. Noting that C' is a constant multiplied by the chain length, it is obtained that the chain length is linearly proportional to the saturation magnetization, in agreement with the experimental results on chain formation obtained by Yusuf [28].

2.2- Field and Concentration Dependence of Magneto-Optical Effects

The results on the field dependences of magneto-optical effects show that a given magneto-optical effect, being birefringence, dichroism, transmission, Faraday rotation or Faraday ellipticity increases sharply and almost linearly with the field at low applied fields, then gradually at intermediate fields approaching saturation at high fields. The degree of polarization, D, of a partially polarized light defined as the ratio of the intensity of the polarized component to the total intensity of light also behaves with the field in a similar manner.

This behavior is assumed to follow a Langiven-type behavior at low concentration (weak interactions) and a modified Langiven behavior at higher concentration of the samples (stronger interactions). This behavior of magneto-optical effects with the field is similar to the behaviors of both magnetization and chain formation. This general trend is explained in terms of two competing effects, the orienting effect (magnetic orientation or physical orientation) of the applied field that tends to align the particles magnetically or physically in the field direction; and the randomizing effect due to thermal agitation which tends to disrupt the alignment in the field direction.

The concentration dependence of most magneto-optical effects was investigated by many workers in the field. All experimental results show that magneto-optical effects increase with the concentration. Furthermore, the results show that samples with higher concentrations saturate at higher fields. Yusuf [78] has investigated the concentration dependence of birefringence and dichroism; and found that both birefringence and dichroism are linear with concentration in the range of concentration (low concentration) used. These results are consistent with the results obtained on chain formation versus concentration. Furthermore they are also in agreement with the theoretical prediction of Fredriq and Houssier [79] for diluted samples.

For Faraday rotation, Faraday ellipticity, the transmission of light and the degree of polarization, nothing is found in the literature to indicate a linear dependence on the concentration of the samples. Furthermore, it is not expected to have such a linear dependence because both Faraday rotation and Faraday ellipticity are affected by the magnetization of the sample as well as by the chain formation.

However, although the transmission of light is not affected by magnetization and is only affected by the chain formation and the reduction of geometrical shadowing of the particles; and because the reduction of the geometrical shadowing may not be linear with concentration, the transmission is found not to be linear with concentration.

Although for low concentration samples, one expects the degree of polarization to increase at least linearly with concentration, the results [70] show that the degree of polarization at a given applied field is not linear with concentration, and most of the values lie below the straight line with slope 1. This may be explained in terms of the depolarization caused by more scattering in samples with higher concentrations due to much larger numbers of particles.

2.3- The Wavelength Dependence of Magneto-Optical Effects

The wavelength dependence of most magneto-optical effects has been investigated by some workers in the field. The wavelength dependence for Faraday rotation, Faraday ellipticity, birefringence, dichroism and the degree of polarization is presented in the next subsections.

2.3.1- Faraday Rotation and Faraday Ellipticity

The wavelength dependence of Faraday rotation and Faraday ellipticity was theoretically studied by Hui and Stroud [62]. Hui and Stroud have presented a theory of Faraday rotation and Faraday ellipticity of a dilute suspension of small particles embedded in a host carrier. They considered the dielectric function of the Faraday active particles to be a complex, frequency-dependant tensor and considered the dielectric function of the host liquid to be a scalar function. Hui and Stroud used the Maxwell-Garnet [63] approximation to calculate the effective dielectric tensor of the suspension in terms of those of the particles and the liquid, and the volume fraction of the particles in the suspension. From the calculated dielectric tensor, they have determined the frequency dependence of Faraday rotation and Faraday ellipticity of the magnetic fluid. Their calculated results for Faraday rotation and Faraday ellipticity are presented in Figs.13 and 14, respectively.

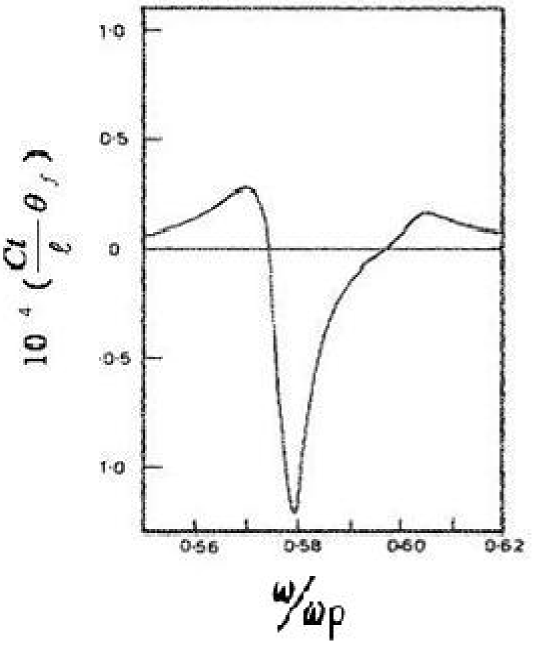

FIG. 13. Faraday rotation versus frequency, normalized to plasma frequency, calculated in [62].

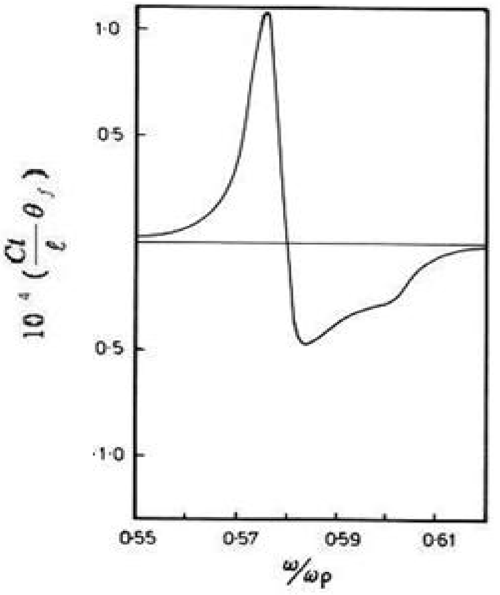

FIG. 14. Faraday ellipticity versus frequency, normalized to plasma frequency, calculated in [62].

Experimentally, the wavelength dependence of Faraday rotation and Faraday ellipticity was investigated by Yusuf and co-workers [64, 65].

The results are presented in Figs.15 and 16, respectively. As can be seen from the Figs.13-16 a good agreement between the calculated and measured results is found. However, the relative width of the resonance in the experimental results is wider than that in the calculated results.

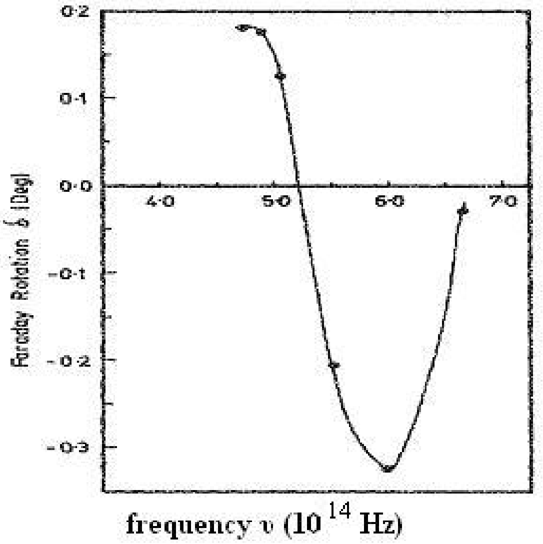

FIG. 15. Faraday rotation versus frequency υ (experimental).

This may be attributed to the fact that in the calculation, Hui and Stroud have only considered mono dispersed spheres of equal size. While in reality the dispersed particles have shape and size distributions. Furthermore, due to the application of an external magnetic field agglomeration and chain formation are bound to occur in the sample. These results seemingly indicate that agglomeration and chain formation play a role in the Faraday rotation and Faraday ellipticity in magnetic fluids.

2.3.2- Birefringence and Dichroism

Llewellen [66] has studied the wavelength dependence of birefringence and dichroism and successfully explained his experimental results in terms of Wiener theory [67] only after taking into account the absorption of light by both the particles and the liquid carrier which is equivalent to considering the dielectric functions to be complex.

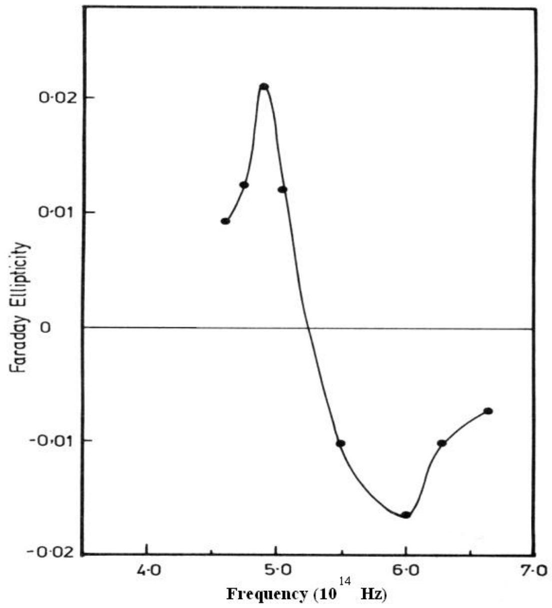

FIG. 16. Faraday ellipticity versus frequency ν (experimental)

Yusuf *et al.* [68] has also investigated the wavelength dependence of birefringence and dichroism in the range of wavelengths (372.5-694.3 nm) and in a magnetic field range (0-500 kA/m). Figs. 17 and 18 show birefringence and dichroism versus field measured at different wavelengths.

Figs. 19 and 20 show birefringence and dichroism versus the wavelength of the electromagnetic waves.

Kooij *et al.* [57] using transmission ellipsometry has investigated the wavelength dependence of birefringence and dichroism but for a narrower range of wavelengths.

Their results are in good agreement with the results of Yusuf *et al.* for the range of wavelengths common in both works.

2.3.3- Degree of Polarization

Polarization effects in magnetic fluids are a consequence of the chain formation in the fluid. Since most magneto-optical effects are dependent on the polarization state of the electromagnetic waves used, it is informative to investigate the polarization effects of magnetic fluids under the application of magnetic fields. The occurrence of chain formation in magnetic fluids, though the chains are irregular in length and thickness, allows for thinking off the sample in terms of a wire grid polarizer. Natural (un-polarized) electromagnetic waves when transmitted through a wire grid emerge partially polarized with a given degree of polarization D.

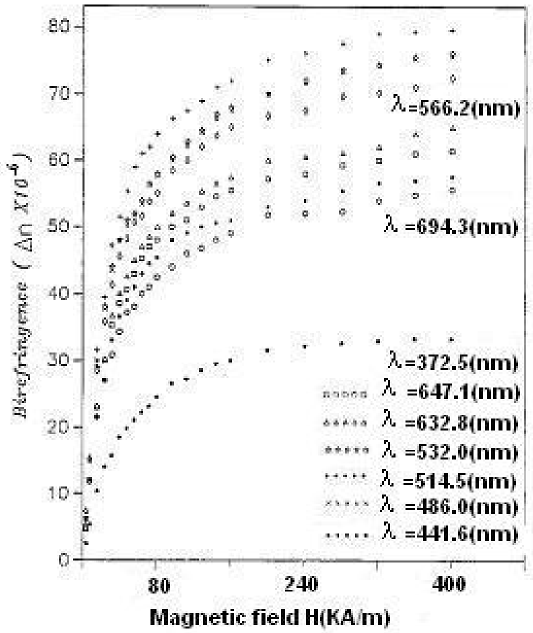

FIG. 17. Birefringence versus measuring field for different wavelengths.

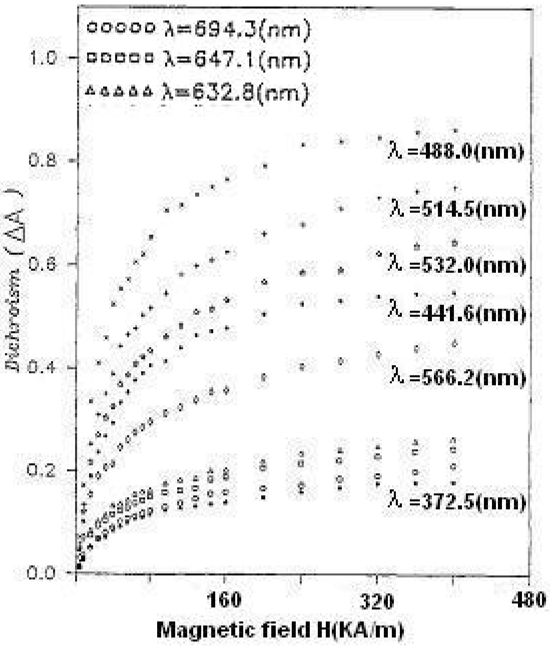

FIG. 18. Dichroism versus measuring field for different wavelengths

The wavelength dependence of the Degree of polarization in magnetic fluids has been investigated by Yusuf *et al.* [70].

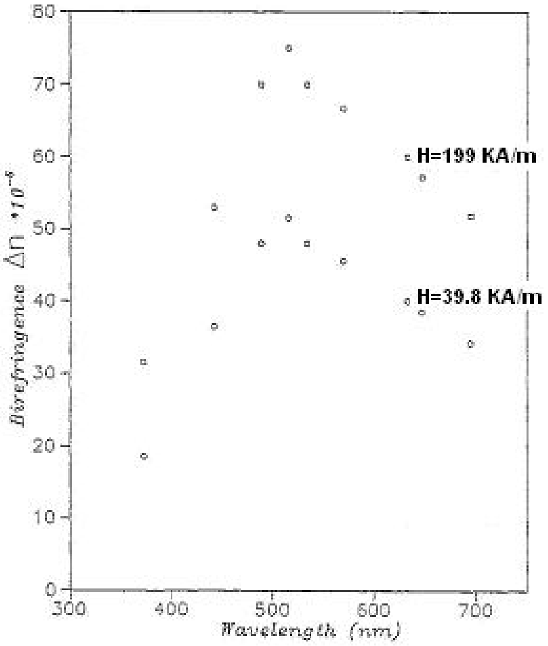

FIG. 19. Birefringence versus wavelength at two measuring field

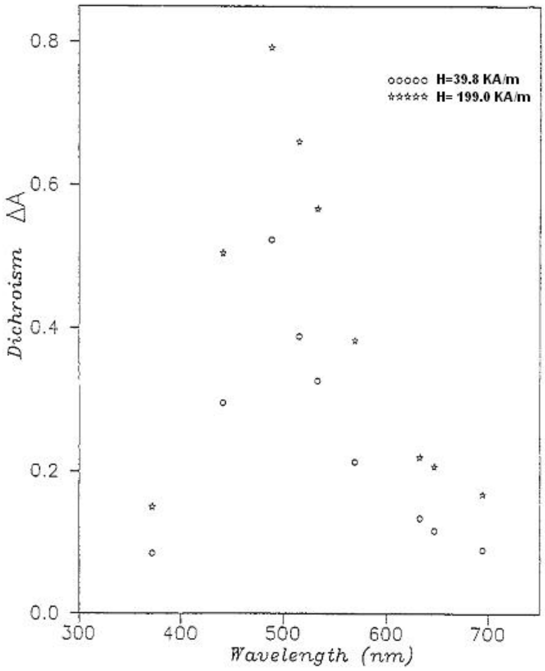

FIG. 20. Dichroism versus wavelength at two measuring field.

Figs. 21 and 22, show the degree of polarization, *D*, measured at different wavelength plotted versus magnetic field for a magnetic fluid sample with $\phi = 1.19 \times 10^{-3}$. The wavelengths λ used in this work ranges between 366- 905 nm [68].

The results show that *D* increases with decreasing wavelength for λ ≥ 488 nm exhibiting a peak at λ = 488 nm and then decreases with further decrease of wavelength

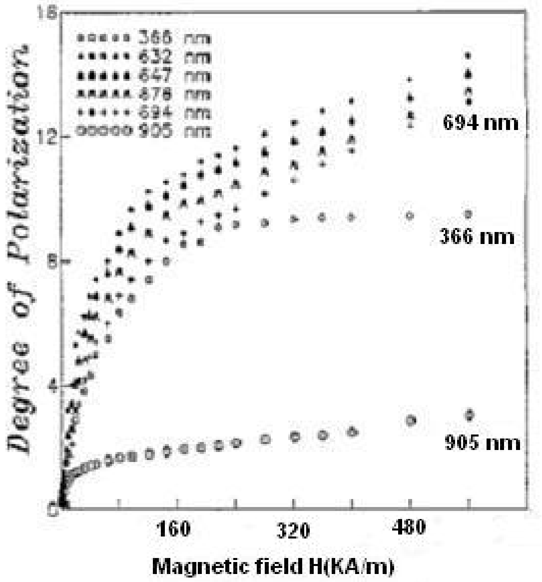

FIG. 21. Degree of polarization versus measuring field for different wavelengths.

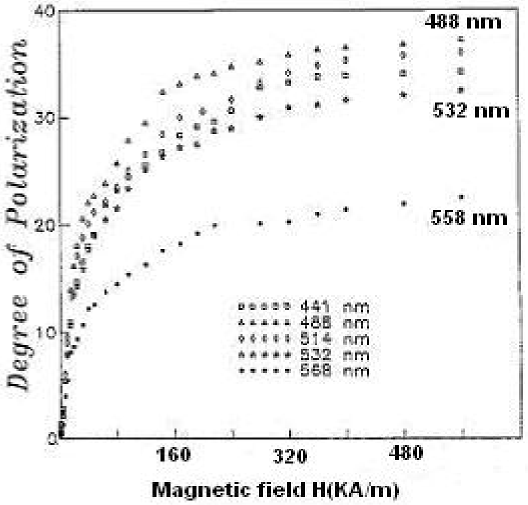

FIG. 22. Degree of polarization versus measuring field for different wavelengths.

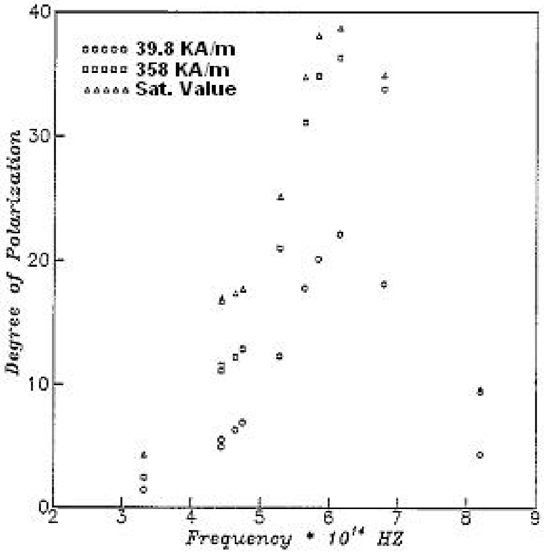

FIG. 23. Degree of polarization measured at various fields versus frequency.

In Fig.23 the degree of polarization is plotted versus frequency. The results show that D increases with frequency for frequencies $\nu < 6 \times 10^{14}$ Hz exhibiting a peak at $\nu = 6 \times 10^{14}$ Hz, then decreases with higher frequencies. The degree of polarization like other magneto-optical effects, exhibits a resonance peak with frequency.

Yusuf and coworkers [68] attributed this behavior to the variation in the absorption of light with electric field vectors parallel and perpendicular to the applied magnetic field with the frequency of the light used; and to the difference in the absorption of these two components. For light propagating normal to the applied magnetic field, the Zeeman interaction results in three lines: a non-shifted ($\nu = \nu_o$) line with its electric field parallel to the applied magnetic field and two shifted lines with their electric fields normal to the applied magnetic field and with frequencies $\nu = \nu_o \pm \Delta\nu$ where $\Delta\nu$ is the change in frequency due to the Zeeman effect. The absorption of these lines peaks at their perspective frequencies, i.e. at ν_o and $\nu_o \pm \Delta\nu$. Fig. 24 shows the three Zeeman lines and their resonance absorptions. Therefore, starting with a frequency $\nu < \nu_o - \Delta\nu$ and by increasing the frequency, the first absorption line at $\nu_o - \Delta\nu$ for the first transverse state is reached and then the transverse component is absorbed more than the longitudinal one resulting in partially polarized light. With further increase in frequency the second absorption line at ν_o for the longitudinal component is reached and then the longitudinal component will be absorbed more than the transverse component, again resulting in partially polarized light. However, it is important to note that the height of the absorption line for the longitudinal component is twice that for the transverse component.

As a result, the degree of polarization increases with frequency in the range $(\nu_o - \Delta\nu) < \nu < \nu_o$ reaching a peak at ν_o. Increasing the frequency above ν_o moves the system away from the absorption line at $\nu = \nu_o$ to third absorption line at $\nu = \nu_o + \Delta\nu$ for the second transverse component, and consequently the degree of polarization decreases.

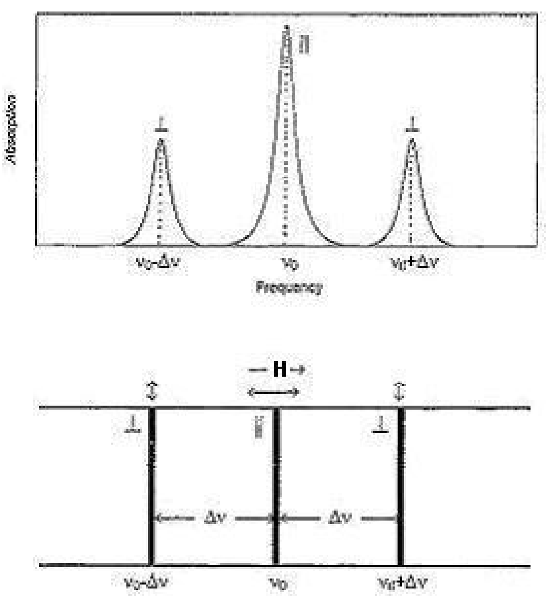

FIG. 24. Zeeman lines and their resonance absorptions.

Although, the Zeeman effect for one single particle, produces partially polarized light, but for an ensemble of randomly oriented particles one expects to have zero degree of polarization as a result of the superposition of a very large number of incoherent light waves partially polarized with their planes of polarization randomly oriented. As the results show, the degree of polarization is zero under zero applied magnetic fields and consequently it is suggested that agglomeration and chain formation play an important role in the polarization effects in magnetic fluids.

2.4- The Temperature Dependence of Magneto-Optical Effects

The temperature dependence of magneto-optical effects was investigated by many workers in the field. This dependence and its investigation have provided more understanding of the origin of magneto-optical effects. Taketomi *et al.* [33-35] has studied the birefringence in the temperature range 290-350 K, well above the melting point of the liquid carrier, and found that birefringence follows a generalized Curie-Weiss type behavior associated with positive ordering temperatures.

Yusuf and co-workers [18-21, 41, 42] have also investigated the temperature dependence of most magneto-optical effects in the temperatures range (100-325 K). This range started from temperatures well below the melting point of the liquid carrier to temperatures well above the melting point of the liquid carrier.

The results of the temperature dependence of Faraday rotation and the transmission of light are presented in Figs. 25 and 26. The results show that below a given temperature (T = 125 K), the transmission of light, dose not change by applying a magnetic field from its value at zero applied field.

However, the Faraday rotation for these temperatures increases linearly with the field. Noting that in this temperature range, the magnetic fluid is in the frozen state and hence the chain formation is physically prohibited, again suggests that the transmission of light is controlled mainly by the chain formation while Faraday rotation has two components one is controlled by the magnetization and the other is due to the chain formation in the fluid. Furthermore, the results show that around 150 K the transmission of light starts to increase with the applied field and that Faraday rotation also starts to increase with the field but not linearly. Above this temperature, both the transmission and Faraday rotation follow Langiven-type behavior with the applied field with values depending on the temperature at which measurements are taken.

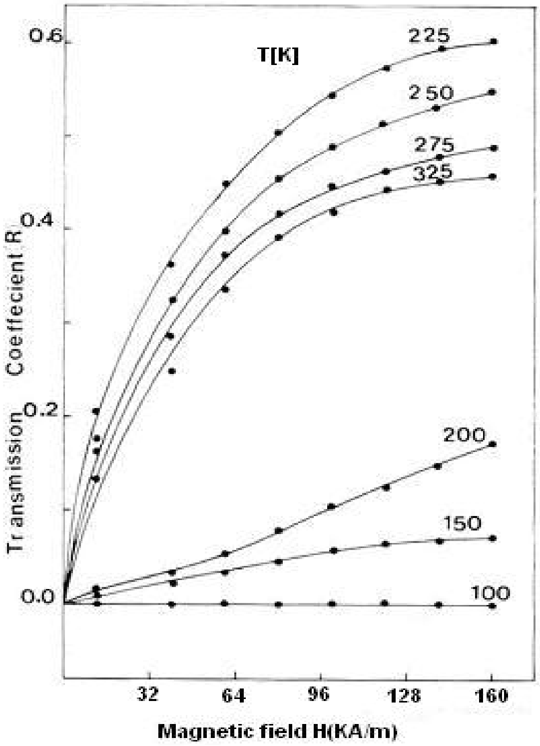

FIG. 25. Transmission versus applied magnetic field at different temperatures.

The results on the temperature dependence of the transmission of light and Faraday rotation are presented in Figs. 27 and 28, respectively. The results show that below 150 K, the change in the transmission of light is zero and Faraday rotation is very weak. For temperatures just above 150 K both the transmission and Faraday rotation increases slowly with temperature and around T = 200 K they both start to increase sharply with temperature exhibiting a cusp-like peak at T = 225 K. Above this temperature both the transmission and Faraday rotation decrease with temperature following a generalized Curie-Weiss type behavior with negative ordering temperatures.

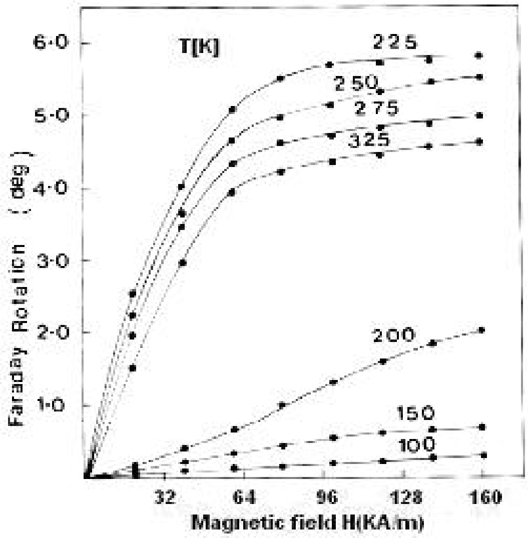

FIG. 26. Faraday rotation versus applied magnetic field at different temperatures.

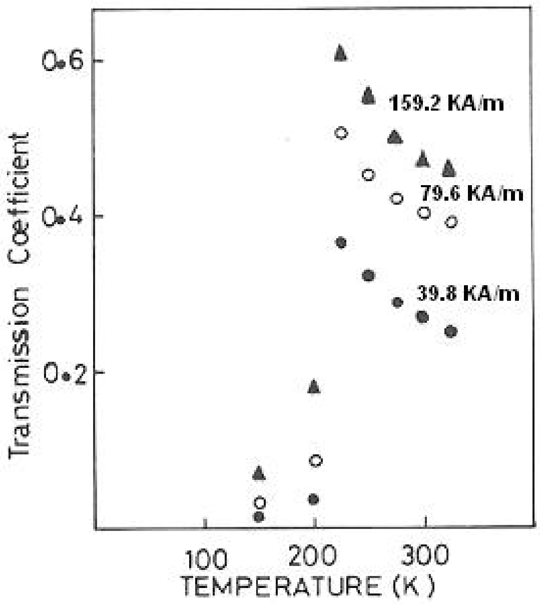

FIG. 27. Transmission versus temperature at different applied magnetic field.

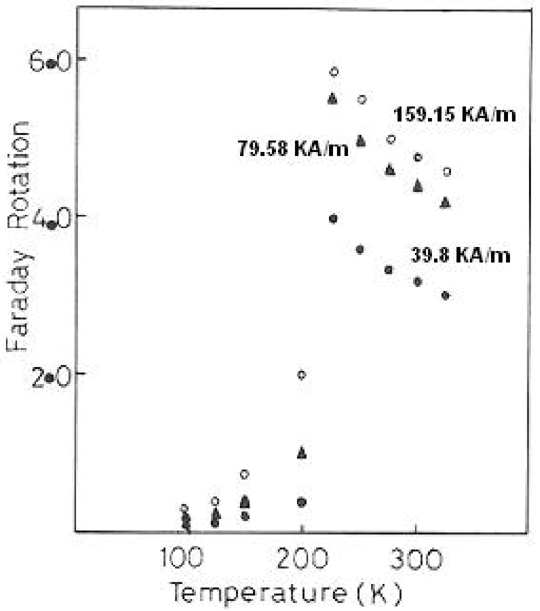

FIG. 28. Faraday rotation versus temperature at different applied magnetic field.

The observation of negative ordering temperatures is in agreement with our magnetic measurements carried on the same samples. They are also in agreement with the results of Popplewell *et al.* [71] obtained for magnetization on Fe_3O_4 magnetic fluid. Studies by Soffge and Schmidbauer [72] indicated a Curie-Weiss type behavior with negative ordering temperatures and have shown two regions of linearity; one at low temperatures yielding a negative ordering temperatures and the other at high temperatures yielding a positive ordering temperatures.

The general temperature dependence of magneto-optical anisotropy effect, i.e., birefringence and dichroism was thoroughly investigated by Yusuf and coworkers [18, 19, 40, and 41] in the temperature range 100-320 K. Both birefringence and dichroism were absent for temperatures lower than ~ 150 K. For temperatures just above 150 K both birefringence and dichroism are detected and with further increase of temperature, sharp increase in both was detected reaching a cusp like maximum at around ~ 200 K. With further increase of temperature both birefringence and dichroism decreases with temperature.

Typical results for the birefringence and dichroism are shown in Figs. 29 and 30. The general temperature dependence of the magneto-optical anisotropy effect will be addressed and discussed in the next section.

Here the Curie-Weiss type behavior will be discussed in connection with the chain formation in the magnetic fluids.

To explain the Curie-Weiss behavior in the magneto-optical effects, Yusuf and co-workers [19] invoked the dependence of these effects on the chain formation and proposed a two-dimensional model based on the Boltzmann distribution. They have assumed that the probability that the magnetic axis of a given particle makes an angle θ with the applied magnetic field follows a Boltzmann distribution, i.e.,

$$P(\theta) = c\exp(\frac{-U}{kT}) \qquad (6)$$

where U is the particle potential energy which consists mainly of two contributions, namely that is due to the applied field and that is due to the dipole-dipole interaction, c is a constant, T is the absolute temperature and k is the Boltzmann constant.

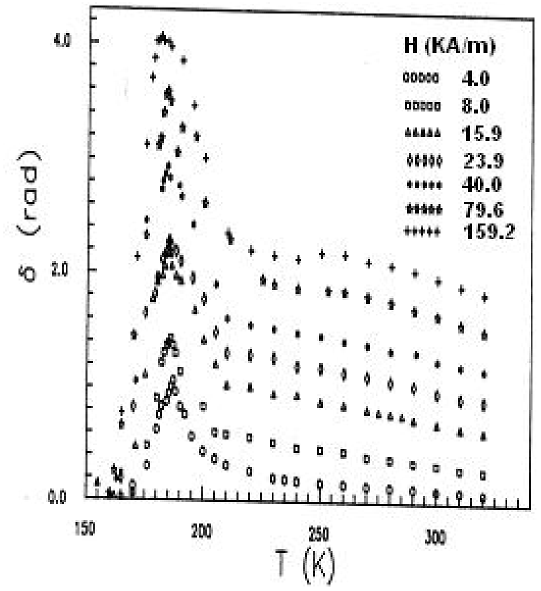

FIG. 29. Birefringence versus temperature at different measuring fields

The number of particles aligned in a given direction is given by the product of the probability $P(\theta)$ and the total number of particles, N in the sample. Hence the effective total chain length, l in a given direction is expressed as follows:

$$l = Nc\bar{d}\,\exp(\frac{-U}{kT}) \tag{7}$$

where $\bar{d}$ is the mean particle diameter.

The chain lengths, $l_{\|}$ parallel to the field direction and, $l_{\perp}$ perpendicular to the field direction are of particular importance in regard to induced magneto-optical anisotropy in magnetic fluids. These two chain lengths for the case of negligible dipole- dipole interactions i.e. in weak samples are given by:

$$l_{\|} = Nc\bar{d}\,\exp(\frac{\mu H}{kT}) \tag{8}$$

And

$$l_{\perp} = Nc\bar{d} \tag{9}$$

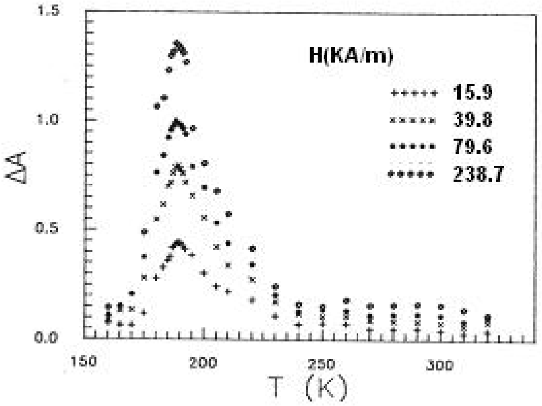

FIG. 30. Dichroism versus temperature at different measuring fields.

The difference in the chain length in the two directions is given by:

$$\Delta l = Nc\bar{d}\{\exp(\frac{\mu H}{kT}) - 1\} \tag{10}$$

and when $\mu H << kT$, it is reduced to:

$$\Delta l = Nc\bar{d}(\frac{\mu H}{kT}) \tag{11}$$

Assuming that the induced birefringence Δn is proportional to Δl, then, the birefringence is, within a constant, given by:

$$\Delta n = \frac{Nc\bar{d}\mu H}{kT} \tag{12}$$

It is seen from Eq. 12 that the birefringence, Δn for high temperature or low fields, follows a Curie type law.

When the intrinsic dipole-dipole interaction is not negligible, Yusuf and co-workers have treated the problem in an analogous way as is usually done in magnetism [70]. It is assumed that due to the chain formation, an internal field, in addition to the externally applied field, is established. This field is assumed to be proportional to the chain length. Consequently the chain lengths parallel and perpendicular to the field direction are expressed as:

$$l_{\|} = Nc\bar{d}\,\exp(\frac{\mu H + \alpha l_{II}}{kT}) \tag{13}$$

and

$$l_{\perp} = Nc\bar{d}\,\exp(\frac{\alpha l_{\perp}}{kT}) \tag{14}$$

Therefore, Δl for a weakly interacting system and $\mu H << kT$, is given by:

$$\Delta l = Nc\bar{d}(\frac{\mu H + \alpha \Delta l}{kT}) \tag{15}$$

Rearrangement of eq. (15) yields the following expression:

$$\Delta l = \frac{Nc\bar{d}\mu H}{k(T - T_o)} \tag{16}$$

with T_o, referred to as ordering temperature, is equal to ($Nc\bar{d}\alpha / k$), consequently the birefringence Δn ,within a constant, is given by:

$$\Delta n = \frac{Nc\bar{d}\mu H}{k(T - T_o)} \tag{17}$$

and hence the birefringence follows a Curie-Weiss type behavior. Therefore, it is believed that the Curie or Curie-Weiss behavior of the magneto-dielectric anisotropy effect in magnetic fluids may be explained in terms of chain formation in the fluid. Furthermore, birefringence Δn as seen from Eq. 12 and Eq. 17 is linearly proportional to the total number of particles, N in the sample which is in turn proportional to the concentration of the sample. Consequently, birefringence is linear with concentration.

The general behavior of the magneto-optical anisotropy effect with temperature has revealed the following basic features [16-19,29, 30]: As is shown in Figs. 29 and 30, magnetic fluids do not exhibit any degree of optical anisotropy below a given temperature

T_S; for $T > T_S$, magnetic fluids start to show some optical anisotropy and the degree of this optical anisotropy increases with temperature reaching a maximum at a temperature T_m; and for $T > T_m$ the degree of the optical anisotropy decreases with temperature. In addition to those basic features it was found that for a given concentration of the magnetic fluid both T_S and T_m decrease with the applied measuring field being the lowest for the highest field as is shown in Figs. 31 and 32 [41, 42].

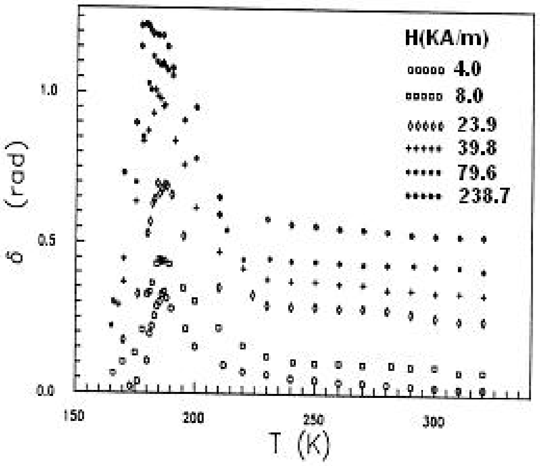

FIG. 31. Birefringence versus temperature at different measuring fields.

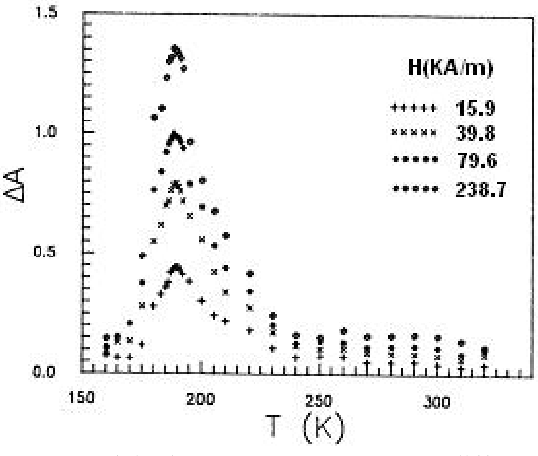

FIG. 32. Dichroism versus temperature at different measuring fields.

It is also found that for a given measuring field both T_S and T_m increase with the concentration of the magnetic fluid being the highest for the highest concentration as is presented in Figs 33 and 36 [41, 42]. Furthermore, it has also been shown that T_m depends on the carrier used in the magnetic fluid [20] such that the lower the viscosity and melting point of the carrier are, the lower T_m is as is seen in Fig. 35.

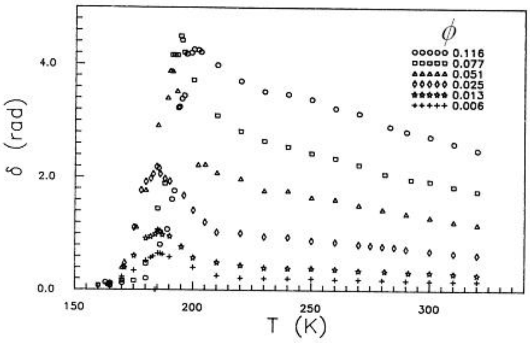

FIG. 33. Birefringence versus temperature for different volumic fractions.

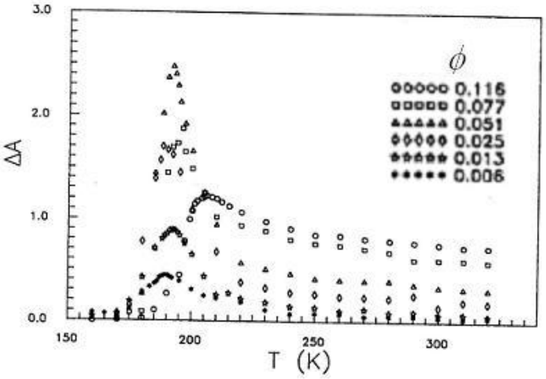

FIG. 34. Dichroism versus temperature for different volumic fractions.

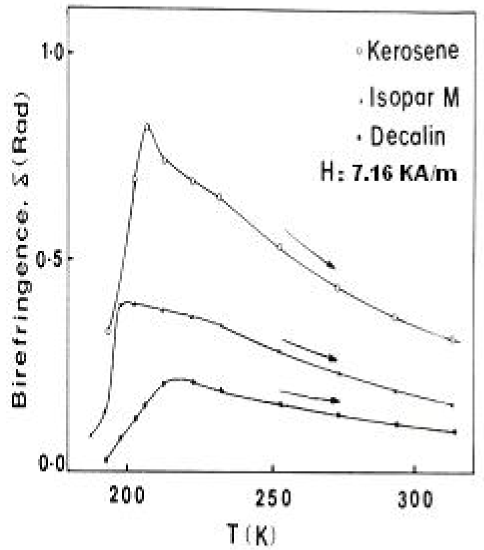

FIG. 35. Birefringence versus temperature at measuring field of 7.16 kA/m for different liquid carriers.

These basic features are basically explained in terms of two competing effects, mainly an orienting effect due to the application of the external field and the randomizing effect due to thermal agitation. Furthermore, as will be shown in the last sections of this article, these basic features have been successfully obtained using numerical calculations based on these two competing effects.

The orienting effect is achieved through either the rotation of the magnetic moments of the particles within the particles while the particles remain fixed in their configuration (Neél relaxation mechanism) or through the physical rotation of the particles while the magnetic moments are fixed in the easy direction of the particles (Brownian relaxation mechanism).

The first mechanism will produce magnetic anisotropy but no mechanical anisotropy in the sample while the second mechanism will produce both mechanical and magnetic anisotropy.

As was stated earlier, the magneto-optical anisotropy effect is mainly due to the induced mechanical anisotropy caused by the agglomeration and chain formation in the sample. Consequently, the magneto-optical anisotropy effect will appear only when the induced mechanical anisotropy is present in the sample. Therefore, it is important to review the mechanism through which the particles will orient themselves with the applied field.

The magnetic moments of the colloidal particles in magnetic fluid may reach thermal equilibrium via two distinct mechanisms. The first is the N$e'el$ relaxation in which the magnetic moments of the particles rotate against the existing anisotropy barrier *ΔE* in a time τ_N given by [36]:

$$\tau_N = [\frac{M_{sb}}{2\alpha\gamma K}][\frac{k_B T}{KV}]^{1/2} \exp(\frac{KV}{k_B T}) \tag{18}$$

where α is an attenuation factor, γ is the gyromagnetic ratio, K is the effective anisotropy constant, V is the magnetic volume of the particle, k_B is the Boltzmann constant, M_{sb} the saturation magnetization of bulk material, and T is the absolute temperature.

The second, mechanism is the Brownian relaxation in which the particles rotate physically so that their easy axes align with the field while the magnetic moments are held fixed in the direction of the easy axis in a time τ_B given by [36]:

$$\tau_B = \frac{3\eta V' s}{k_B T} \tag{19}$$

where η is the viscosity of the magnetic fluid, V' is the hydrodynamic volume of the particle and s is a geometrical factor (s = 1 for spherical particles).

The dominant relaxation mechanism is the one with the shorter relaxation time. As can be seen from Eq. 28 the N$e'el$ relaxation time grows exponentially with the magnetic volume, therefore, only small particles may relax via the N$e'el$ relaxation mechanism.

In magnetic fluids, there is always a size distribution of the particles, consequently a volume for which $\tau_N = \tau_B$ exists. This volume is known as the Shliomis volume, V_s [36, and 37].

Only particles with $V > V_s$ will relax via the Brownian mechanism, thus contributing to the optical anisotropy. It is, therefore, necessary to determine the Shliomis volume, V_s. This is accomplished by equating the two relaxation times and assuming $V = V'$ yielding the following transcendental relation:

$$q^{-3/2} \exp(q) = \frac{6\alpha\gamma\eta}{M_{sb}} \tag{20}$$

where $q = (KV/k_B T)$. The relation in Eq. 20 is numerically solved for the Shliomis volume, V_s. As seen from this equation, the viscosity, η, is the determining factor for the Shliomis volume at a given temperature and therefore it is necessary to state some relations related to the viscosity of a magnetic fluid.

It is well established that the viscosity of a magnetic fluid varies with the concentration of the magnetic particles, the applied field, temperature and inter-particle interactions. The viscosity of a non-aggregating, highly diluted (ϕ << 0.1) colloidal suspension is approximated by the Einstein formula [37]:

$$\eta = \eta_o (1 + 2.5\phi) \tag{21}$$

where η_o is the viscosity of the liquid carrier and. ϕ is the concentration of the sample. For ϕ ~ 0.1, the viscosity starts to deviate from linearity and for ϕ = 0.3 the viscosity increases sharply with a pronounced nonlinear behavior.

The exact functional dependence of the viscosity on temperature is not well defined, but for a qualitative discussion the viscosity (may be expressed as [39, 40]:

$$\ln(\frac{\eta}{\eta_o}) = \frac{B}{T - T_o} \qquad T \approx T_o \tag{22}$$

$$\ln(\frac{\eta}{\eta_o}) = \frac{B'}{T^n} \qquad T > T_o \tag{23}$$

where B and B' are characteristic positive constants, T_o is a temperature below the melting point of the colloid, and n is a constant, usually taken to be larger than one.

For a colloidal suspension, Eq. 23 will be applied in the liquid region.

It is relevant to mention that the viscosity of magnetic fluids depends not only on the applied magnetic field but also on its direction [36].

It is worth mentioning that at low fields the transverse and longitudinal components of the magnetization have the same relaxation time which is τ_B. For high fields, however, the relaxation time for the longitudinal component is still equal to τ_B, while that for the transverse component $\tau_\perp$ is given by [38]:

$$\tau_\perp = \frac{2\tau_B}{p} \tag{24}$$

where $p = \mu_o M_{sb} VH / k_B T$

The magnetic particles in the fluid may have intrinsic optical anisotropy due to their anisotropic shapes, although the magnetic fluid under zero fields will have no optical anisotropies due to the random orientation of the particles in the fluid. When an external magnetic field is applied to the fluid, induced optical anisotropy results as a consequence of the orientation of the particles and to the field induced chain formation.

The optical anisotropy of a uniaxial single-domain particle suspended in a nonmagnetic liquid carrier under the application of an external magnetic field was treated by Hartmann and Mende [16, 17] and Scholten [14, 15]. In a carrier liquid with isotropic, real refractive index n_o this optical anisotropy is given by [14-17]

$$\Delta\tilde{n}(T,H) = \frac{2\kappa\varepsilon}{n_o}(\tilde{g}_a - \tilde{g}_b)\Phi(p,q) \tag{25}$$

where $\tilde{g}_a$ and $\tilde{g}_b$ are the complex polarizabilities of the magnetic particles, which are usually given as:

$$\tilde{g}_i = \frac{\tilde{n}_p^2 - \tilde{n}_o^2}{1 + \{(\tilde{n}_p^2 - \tilde{n}_o^2)N_i / \tilde{n}_o^2\}} \tag{26}$$

where $\tilde{n}_p$ is the anisotropic refractive index of the particle, and N_i is the demagnetization coefficient which depends only on the axial ratio (a/b) of the particle. $\Phi(p,q)$, is an orientation function usually expressed as a product of two functions, i.e.

$$\Phi(p,q) = \xi(q) f(p) \tag{27}$$

where $\xi(q)$ represents the coupling between the magnetic moment of the particle and its easy axis and is usually expressed as:

$$\xi(q) = \frac{3}{4q}(\frac{q^{1/2}\exp(q) - I(q)}{I(q)}) - \frac{1}{2} \tag{28}$$

where

$$I(q) = \int_o^{\sqrt{q}} \exp(x^2)dx \tag{29}$$

The function $f(p)$ is given by:

$$f(p) = [1 - \frac{3L(p)}{p}] \tag{30}$$

where $L(p)$ is the Langevin function, and $p = \mu_o M_{sb} VH / k_B T$.

The birefringence, Δn and dichroism, ΔA, are obtained from the real and imaginary parts of the optical anisotropy, $\Delta\tilde{n}$, i.e.,

$$\Delta n = \frac{2\kappa\varepsilon}{n_o}\mathrm{Re}(\tilde{g}_a - \tilde{g}_b)\Phi(p,q) \tag{31}$$

And

$$\Delta A = \frac{2\kappa\varepsilon}{n_o}\mathrm{Im}(\tilde{g}_a - \tilde{g}_b)\Phi(p,q) \tag{32}$$

When the particle size distribution is taken into consideration, the total birefringence, Δn_T, and total dichroism ΔA_T will be given by:

$$\Delta n_T = \int_{V_s}^{\infty} \Delta n F(V) dV \tag{33}$$

and

$$\Delta A_T = \int_{V_s}^{\infty} \Delta A F(V) dV \tag{34}$$

where $F(V)$ is a suitable particle size distribution often taken as a log-normal distribution, and V_s, is the Shliomis volume which is obtained by solving Eq. 20 numerically.

The basic features observed for the magneto-optical anisotropy effect against temperature are explained as follows: For temperatures below T_S, the magnetic fluid is in the frozen state with infinite viscosity and hence the particles are blocked against the physical rotation resulting in no mechanical anisotropy in the sample and consequently the absence of the magneto-optical anisotropy. When the temperature reaches, T_S, (the slurry state temperature) some of the particles are unblocked and orient themselves in the field direction producing some degree of mechanical anisotropy and as a result magneto-optical anisotropy appears. Increasing the temperature near T_S results in a sharp decrease in the viscosity of the sample allowing more particles, in large numbers, to be unblocked and orient themselves in the field direction and thus an increase not only in the number of chains but also in their lengths leading to sharp enhancement of the optical anisotropy. Further increase of temperature still results in reducing the viscosity of the sample and thus increases the chances for unblocking the particles. But increasing the temperature has also another effect that is a randomizing effect which results in disorienting the particles and thus in reducing the optical anisotropy.

It is the competition between these two effects that determines whether the optical anisotropy will increase or decrease. For temperatures above T_S and below some temperature T_m the unblocking effect is the dominant one and the optical anisotropy increases till it reaches a maximum at T_m. By increasing the temperature above T_m the balance is disturbed and the randomizing effect becomes more effective though the unblocking effect still plays a role but with smaller number of particles. As a result the optical anisotropy starts to decrease with temperature for $T > T_m$.

Increasing the measuring magnetic field increases the magnetic torque exerted on each particle in the sample and consequently the particle will be able to rotate against a higher viscous torque, *i*.e., at a lower temperature than that for a weaker applied field. Hence the unblocking of particles starts at a lower temperature, and the optimum condition (temperature) will be lower. Therefore, the temperatures at which the onset and the maximum of the optical anisotropy, occur, decrease with increasing the applied magnetic field.

Increasing the concentration of sample, results in increasing both the viscosity and the melting point of the sample. It is obvious that increasing the viscosity and melting point of the sample results in increasing both T_S and T_m.

Using liquid carriers having different initial viscosities leads to changing the position of both T_S and T_m such that the lower the initial viscosity is the lower both these two temperatures are.

The arguments that would be used to explain the effect of concentration and viscosity on the position of T_S and T_m are similar to those used to explain the effect of the measuring field.

3-Magneto-Dielectric Anisotropy Effects in Magnetic Fluids

The magneto-dielectric effect in magnetic fluids has been investigated by many workers both experimentally and theoretically [43-53]. The experimental investigations were based on impedance measurement techniques where the magnetic fluid is placed in a capacitor. Measurements of the impedance parameters such as the modulus and phase are carried out using a bridge or an RLC meter [43-50]. It is known that impedance measurement techniques suffer some serious disadvantages such as electrode effects, parasitic impedances, skin depth and accuracy-related problems.

On the theoretical side, Monte Carlo simulations were used to calculate the magneto-dielectric effect [51-53].

Stroud and co-workers [62] have calculated some magneto-optical effects (Faraday rotation and Faraday ellipticity) by determining the dependence of the off-diagonal elements of the permittivity tensor on field, temperature and frequency. Their findings were experimentally verified by Yusuf and coworkers [64, 65].

Using the opposite approach Llewellyn [66] has calculated the elements of the skew symmetric permittivity tensor of $Fe_3 0_4$ particles from their simultaneous measurements of birefringence, dichroism, Faraday rotation and Faraday ellipticity in $Fe_3 0_4$ particle magnetic fluids.

Yusuf and co-workers [68, 69] have calculated the magneto-dielectric anisotropy effect in magnetic fluids from the optical anisotropy (i.e. birefringence and dichroism) measurements. They have investigated the field, concentration, Temperature and wavelength dependence of the magneto-dielectric anisotropy effect. Both the real and imaginary parts of the dielectric constant seen by light polarized parallel or perpendicular to the external magnetic field are calculated.

Determining the magneto-dielectric anisotropy effects using optical anisotropy measurements has the advantage over the conventional method in that it is highly accurate and is not affected by electrode effects or skin depth and parasitic impedances.

The dielectric constant of a magnetic fluid in the absence of an external magnetic field exhibits no anisotropy due to the random orientation of the particles. Therefore, the dielectric constant seen by light with different states of polarization is the same. However, when a magnetic field is applied, orientation of particles and field-induced chain formation in the field direction take place leading to two different average lengths $l_{\|}$ in the field direction and $l_{\perp}$ perpendicular to the field direction; consequently the dielectric constant will exhibit some degree of anisotropy.

The magneto-dielectric anisotropy factor $g(H,\omega)$ is defined as:

$$g(H,\omega)=\frac{\varepsilon_{\|}(H,\omega)-\varepsilon_{o}(0,\omega)}{\varepsilon_{o}(0,\omega)-\varepsilon_{\perp}(H,\omega)} \quad (35)$$

The value of this factor obtained by different investigators was either 1 or 2 depending on the sample investigated [45, 48, 49, 50]. Using their magneto-optical measurements, Yusuf and coworkers [68, 69] have shown that $g = 1$ for thin samples (2-dimensional case) and that $g = 2$ for thick samples (3-dimensional case).

3.1- Derivation of Fundamental Equations

In general, the dielectric constant of the magnetic fluid is complex and is written as:

$$\tilde{\varepsilon}=\varepsilon'-i\varepsilon'' \quad (36)$$

where ε' and ε'' are the real and imaginary parts of the dielectric constant, respectively. Furthermore, the index of refraction of the fluid is also complex and is written as:

$$\tilde{n}=n-ik \quad (37)$$

where n and k are the real index of refraction and the extinction coefficient, respectively.

Conventionally, the dielectric constant and the index of refraction are related by:

$$\tilde{\varepsilon}=\tilde{n}^2=n^2-k^2-2ink \quad (38)$$

When an external magnetic field is applied, the dielectric constant $\tilde{\varepsilon}$ becomes anisotropic, thus exhibiting two different behaviors for light polarized parallel to the magnetic field direction $\tilde{\varepsilon}_{\|}$ and to that polarized perpendicular to the magnetic field $\tilde{\varepsilon}_{\perp}$. Similarly, the index of refraction exhibits two indices $\tilde{n}_{\|}$, $\tilde{n}_{\perp}$, and the extinction coefficient also exhibits two values $k_{\|}$, $k_{\perp}$.

Accordingly, Eq. (38) will be modified such that it incorporates this induced anisotropy. The modified equations are:

$$\tilde{\varepsilon}_{\|} = \varepsilon'_{\|} - i\varepsilon''_{\|} = n_{\|}^2 - k_{\|}^2 - 2in_{\|}k_{\|} \qquad (39)$$

and

$$\tilde{\varepsilon}_{\perp} = \varepsilon'_{\perp} - i\varepsilon''_{\perp} = n_{\perp}^2 - k_{\perp}^2 - 2in_{\perp}k_{\perp} \qquad (40)$$

By equating the real and imaginary parts in equation (39) and in equation (40), the following equations are obtained:

$$\varepsilon'_{\|} = n_{\|}^2 - k_{\|}^2 \qquad (41a)$$

$$\varepsilon''_{\|} = 2n_{\|}k_{\|} \qquad (41\ b)$$

and

$$\varepsilon'_{\perp} = n_{\perp}^2 - k_{\perp}^2 \qquad (42\ a)$$

$$\varepsilon''_{\perp} = 2n_{\perp}k_{\perp} \qquad (42\ b)$$

The distinction between a two dimensional (thin) system and a three dimensional (thick) system is manifested in the relation joining $n_{\|}$, $n_{\perp}$ and n_o; $k_{\|}$, $k_{\perp}$, and k_o; where n_o and k_o are the index of refraction and extinction coefficient of the sample, at zero fields, respectively.

For a two dimensional system Yusuf and coworkers [68] used the following relations:

$$n_{\|} + n_{\perp} = 2n_o \qquad (43a)$$

and

$$k_{\|} + k_{\perp} = 2k_o \qquad (43b)$$

However for a three dimensional sample they [66] used the following equations:

$$n_{\|} + 2n_{\perp} = 3n_o \qquad (44a)$$

and

$$k_{\|} + 2k_{\perp} = 3k_o \qquad (44b)$$

And by using the definition of birefringence and dichroism expressed as:

$$\Delta n = n_{\|} - n_{\perp} \qquad (45a)$$

and

$$\Delta k = k_{\|} - k_{\perp} \qquad (45b)$$

One gets the two sets of equations, the first set is applicable to the two dimensional sample and consists of the four following equations:

$$\varepsilon'_{\|} = (n_o + \frac{\Delta n}{2})^2 - (k_o + \frac{\Delta k}{2})^2 \qquad (46a)$$

$$\varepsilon''_{\|} = 2(n_o + \frac{\Delta n}{2})(k_o + \frac{\Delta k}{2}) \qquad (46b)$$

$$\varepsilon'_{\perp} = (n_o - \frac{\Delta n}{2})^2 - (k_o - \frac{\Delta k}{2})^2 \qquad (46c)$$

$$\varepsilon''_{\perp} = 2(n_o - \frac{\Delta n}{2})(k_o - \frac{\Delta k}{2}) \qquad (46d)$$

while the second set is applicable to the three dimensional sample and consists of the following equations:

$$\varepsilon'_{\|} = (n_o + \frac{2\Delta n}{3})^2 - (k_o + \frac{2\Delta k}{3})^2 \qquad (47a)$$

$$\varepsilon''_{\|} = 2(n_o + \frac{2\Delta n}{3})(k_o + \frac{2\Delta k}{3}) \qquad (47b)$$

$$\varepsilon'_{\perp} = (n_o - \frac{\Delta n}{3})^2 - (k_o - \frac{\Delta k}{3})^2 \qquad (47c)$$

$$\varepsilon''_{\perp} = 2(n_o - \frac{\Delta n}{3})(k_o - \frac{\Delta k}{3}) \qquad (47d)$$

The last two sets of equations are the fundamental equations for calculating the magneto-dielectric anisotropy effect. They show that magneto-dielectric effects can be determined from optically measured physical quantities such as birefringence Δn, dichroism ΔA, the real refractive index n_o, and the extinction coefficient k_o (under zero applied fields). It is important to mention that these physical quantities can be measured with excellent accuracies, e.g. values of Δn and $\Delta k \sim 10^{-6}$ can easily be measured.

The frequency dependence of the index of refraction, or the dielectric constant of matter (dispersion), is explained in terms of the distortion of the internal charge distribution under the influence of an applied external electric field. This distortion results in induced electric dipole moments leading to an induced- electric polarization. Considering the charge carriers to be elastically bound, the electric field of the electromagnetic wave provides the driving force of the harmonic oscillator. Following standard procedures for solving the equation of a forced damped oscillator, the dielectric constant is given by:

$$\tilde{\varepsilon} = \varepsilon_o + \frac{q^2 N}{m(\omega_o^2 - \omega^2 + i\gamma\omega)} \tag{48}$$

where ε_o is the dielectric constant of free space, q the charge of the charge carriers, N the number of free charge carriers per unit volume, m the mass of the charge carrier, ω_o the natural frequency of the oscillator, ω the frequency of the electromagnetic wave and γ a damping parameter.

For an elongated particle, the charge carriers can oscillate along the easy direction much easier than along other directions and with larger amplitudes leading to more electric polarization in the easy direction. Therefore, the contribution to the dielectric constant of charge carriers oscillating along the easy axis is the dominant one. When a magnetic field is applied on the sample, the number of charge carriers, N, contributing to the dielectric constant becomes direction dependant, thus leading to an induced anisotropy in the dielectric constant of the sample. Consequently, the dielectric constant of the sample under an applied magnetic field is given by:

$$\tilde{\varepsilon}_x = \varepsilon_o + \frac{q^2 N_x}{m(\omega_o^2 - \omega^2 + i\gamma\omega)} \tag{49}$$

$$\varepsilon_y = \varepsilon_o + \frac{q^2 N_y}{m(\omega_o^2 - \omega^2 + i\gamma\omega)} \tag{50}$$

and,

$$\tilde{\varepsilon}_z = \varepsilon_o + \frac{q^2 N_z}{m(\omega_o^2 - \omega^2 + i\gamma\omega)} \tag{51}$$

where $\tilde{\varepsilon}_x$, $\tilde{\varepsilon}_y$, and $\tilde{\varepsilon}_z$ are the complex dielectric constants seen by the electromagnetic waves polarized in the x, y, and z directions respectively; and N_x, N_y and N_z are the number of charge carriers per unit volume oscillating in the x, y, and z directions respectively.

In the absence of applied magnetic fields the densities of charge carriers oscillating in the three directions are equal and thus N_x = N_y = $N_z = (1/3)N$, where N is the density of charge carriers in the sample. Therefore, $\tilde{\varepsilon}_x$, $\tilde{\varepsilon}_y$ and $\tilde{\varepsilon}_z$ are all equal to $\tilde{\varepsilon}_{ze}$ (dielectric constant under zero magnetic fields) and given by:

$$\tilde{\varepsilon}_x = \tilde{\varepsilon}_y = \tilde{\varepsilon}_z = \varepsilon_o + \frac{q^2 N}{3m(\omega_o^2 - \omega^2 + i\gamma\omega)} \tag{52}$$

When a magnetic field H is applied in the z direction, the particles tend to align in the field direction with a probability $P(T,H)$ given by:

$$P(T,H) = \frac{1 + 2\Phi(p,q)}{3} \tag{53}$$

where $\Phi(p,q)$ is the orientation function previously defined. This expression for the probability insures that it is (1/3) at zero field or very high temperatures and is 1 at very high fields or very low temperatures.

Furthermore, the probability $P(T,H)$ at a given field and given temperature is the same for samples of different concentration in the low concentration case where particle-particle interaction is neglected. The densities of charge carriers are then given by:

$$N_z = NP(T,H) \tag{54}$$

$$N_x = N_y = N\frac{1 - P(T,H)}{2} \tag{55}$$

By substituting N_x and N_z in Eq. (49) and Eq. (51), one gets the following expressions for the dielectric constant:

$$\tilde{\varepsilon}_{\parallel} = \varepsilon_o + \frac{q^2 NP(T,H)}{m(\omega_o^2 - \omega^2 + i\gamma\omega)} \tag{56}$$

$$\tilde{\varepsilon}_{\perp} = \varepsilon_0 + \frac{q^2 N\{1 - P(T,H)\}}{2m(\omega_o^2 - \omega^2 + i\gamma\omega)} \tag{57}$$

And by separating the real and imaginary parts in Eq. (56), Eq. (57) one obtains the following relations:

$$\varepsilon'_{\parallel} = \varepsilon_o + f_1(\omega)NP(T,H) \tag{58}$$

$$\varepsilon'_{\perp} = \varepsilon_o + \frac{f_1(\omega)N(1 - P(T,H))}{2} \tag{59}$$

$$\varepsilon''_{\parallel} = f_2(\omega)NP(T,H) \tag{60}$$

$$\varepsilon''_{\perp} = \frac{f_2(\omega)N\{1 - P(T,H)\}}{2} \tag{61}$$

$$\varepsilon'_{ze} = \varepsilon_o + \frac{Nf_2(\omega)}{3} \tag{62}$$

$$\varepsilon''_{ze} = \frac{Nf_2(\omega)}{3} \tag{63}$$

where $f_1(\omega)$ and $f_2(\omega)$ are given by:

$$f_1(\omega) = \frac{\gamma\omega q^2}{m\{(\omega_o^2 - \omega^2)^2 + (\gamma\omega)^2\}} \tag{64}$$

$$f_2(\omega) = \frac{(\omega_o^2 - \omega^2)q^2}{m\{(\omega_o^2 - \omega^2)^2 + (\gamma\omega)^2\}} \tag{65}$$

The field-induced change in the real dielectric constants and that in the imaginary dielectric constant are then given by:

$$\Delta\varepsilon'_{\|} = f_1(\omega)N\{P(T,H) - \frac{1}{3}\} \tag{66}$$

$$\Delta\varepsilon'_{\perp} = \frac{1}{2}f_1(\omega)N\{\frac{1}{3} - P(T,H)\} \tag{67}$$

$$\Delta\varepsilon''_{\|} = f_2(\omega)N\{P(T,H) - \frac{1}{3}\} \tag{68}$$

$$\Delta\varepsilon''_{\perp} = \frac{1}{2}f_2(\omega)N\{\frac{1}{3} - P(T,H)\} \tag{69}$$

At a given frequency, ω, both $f_1(\omega)$ and $f_2(\omega)$ are constant and consequently, the field induced change in the real and imaginary parts of dielectric constant (at a given measuring field and temperature) in the low concentration regime is linear with the density number N and thus is linear with concentration. The slope of this linear relationship is positive for the change in the dielectric constant, (real and imaginary parts) for waves polarized in the field direction and is negative for the change in the dielectric constant, (real and imaginary parts) for those polarized normal to the field direction. However, for a given sample, the field induced change in the real and imaginary parts of dielectric constant is field dependent since $P(T,H)$ is field dependent. The change in the dielectric constant, (real and imaginary parts) for waves polarized in the field direction is positive and increases with the field while this change for those polarized normal to the field direction negative and its absolute value increases with the field.

3.2- Field Dependence of the Dielectric Anisotropy

Using the first set of equations, *i.e.* Eq.46 (two-dimensional case) and the data on birefringence and dichroism presented in reference [68] and the measured values n_o and k_o of the sample, the dielectric constants $\varepsilon_{\|}$ and $\varepsilon_{\perp}$ both the real and imaginary parts were calculated versus field. The results of these calculations are presented in Figs. 36 and 37.

The results in Figs. 36 and 37 show that at zero fields both $\varepsilon_{\|}$ and $\varepsilon_{\perp}$ are equal. Applying magnetic fields on the sample results in a “forking behavior”, *i.e.,* an increase in both the real and imaginary parts of $\varepsilon_{\|}$ and a decrease in both the real and imaginary parts of $\varepsilon_{\perp}$. This forking effect is attributed to the chain formation in the direction of applied field. It is important to note that at any given applied field the two differences ($\varepsilon_{\|}$ - ε_o) and (ε_o - $\varepsilon_{\perp}$) are equal and thus yield the value of 1 for the dielectric anisotropy factor g. These results are consistent with the theory presented in Eqs. 66-69.

Similarly, the change in the dielectric constant from the measured values of birefringence and dichroism for different samples at room temperature and wavelength of 633 nm, and the measured values of n_o and k_o, was calculated for a three dimensional case using Eq. 47. The results are presented in Figs. 38 and 39.

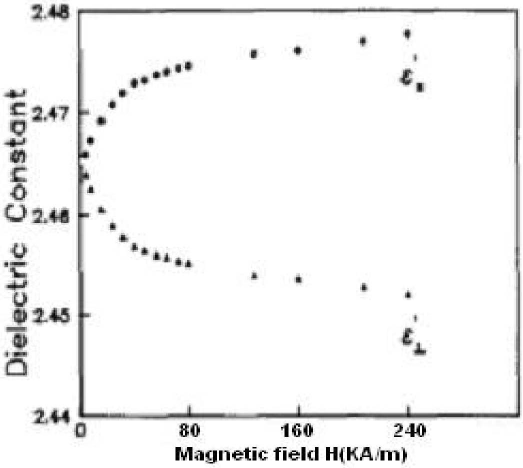

FIG. 36. Real parts $\varepsilon'_{\|}$ and $\varepsilon'_{\perp}$ of the dielectric constant versus applied magnetic field.

The results show similar behavior with the field to that for the two-dimensional case, but with one fundamental difference, that is the change in the dielectric constant for waves polarized in the field direction is twice the change (in absolute value) for waves polarized normal to the field direction. Therefore, the dielectric anisotropy factor, g, is 2 for the three dimensional case.

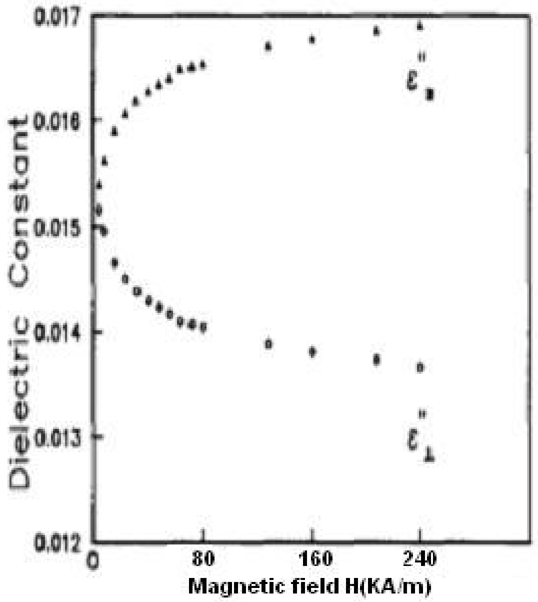

FIG. 37. Imaginary parts $\varepsilon''_{\parallel}$ and $\varepsilon''_{\perp}$ of the dielectric constant versus applied magnetic field.

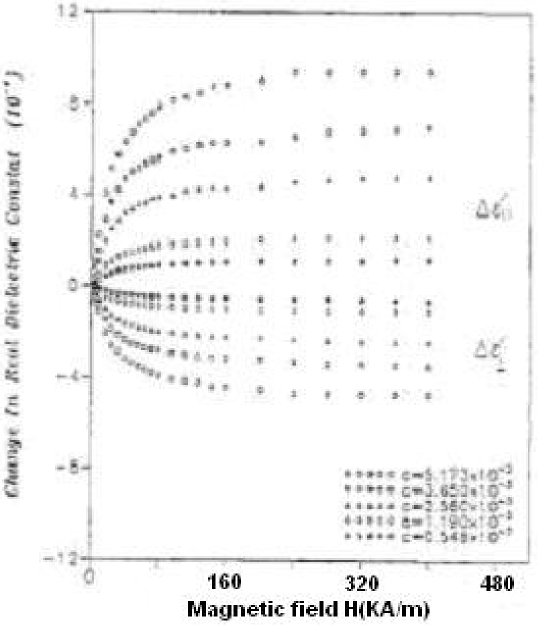

FIG. 38. Field induced changes $\Delta\varepsilon'_{\parallel}$ and $\Delta\varepsilon'_{\perp}$ versus applied magnetic field for different concentrations and $\lambda = 633$ nm.

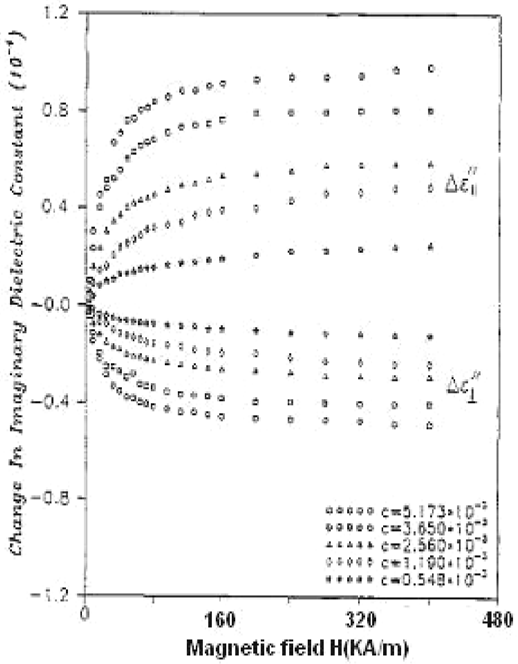

FIG. 39. Field induced changes $\Delta\varepsilon''_{\parallel}$ and $\Delta\varepsilon''_{\perp}$ versus applied magnetic field for different concentrations and $\lambda = 633$ nm.

3.3- Concentration Dependence of the Dielectric Anisotropy

The concentration dependence of the dielectric anisotropy is calculated from the measured values of birefringence and dichroism for different samples taken at a given field and room temperature and wavelength of 633 nm; and the measured values of n_o and k_o of these samples. The calculations were for a three dimensional sample, *i.e.* using Eq. 47.

The results of these calculations for the change in the dielectric constant, both real and imaginary parts are presented in Fig. 40 and Fig. 41.

The results show that the change in the dielectric constant (real and imaginary parts) for waves polarized in the field direction increases linearly with concentration; while this change for those polarized normal to the field direction decreases linearly with concentration.

Noting that the concentrations of the samples used are in the low concentration regime, this linearity is in agreement with the theory presented in Eqs. 66- 69. Furthermore, the results also show that, for all concentrations, the dielectric anisotropy factor g is 2.

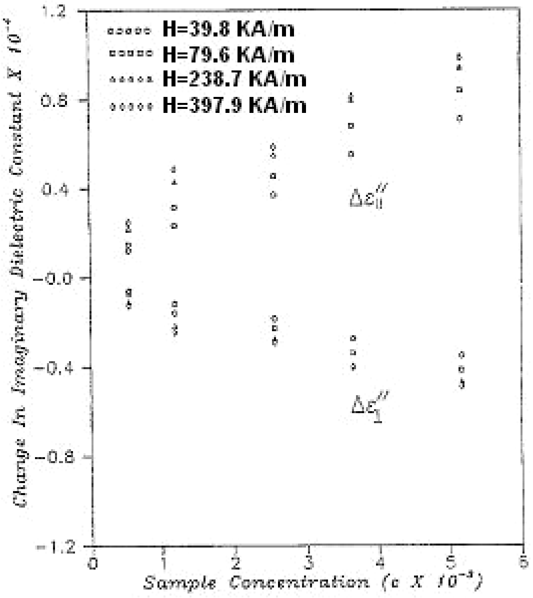

FIG. 40. Field induced changes $\Delta\varepsilon''_{\parallel}$ and $\Delta\varepsilon''_{\perp}$ versus concentrations for different applied magnetic field and $\lambda = 633$ nm

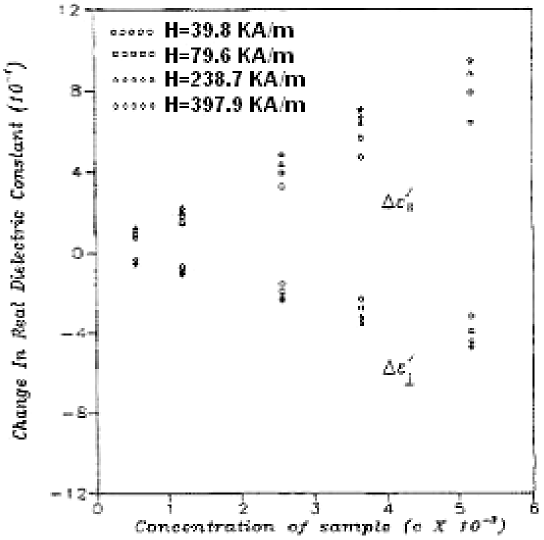

FIG. 41. Field induced changes $\Delta\varepsilon'_{\parallel}$ and $\Delta\varepsilon'_{\perp}$ versus concentrations for different applied magnetic field and $\lambda = 633$ nm

3.4- Temperature Dependence of the Dielectric Anisotropy

The temperature dependence of the magneto dielectric anisotropy was calculated for a two dimensional case using measurements of birefringence and dichroism as a function of temperature and the measured values of n_o and k_o. The results of these calculations are shown in Figs. 42 and 43.

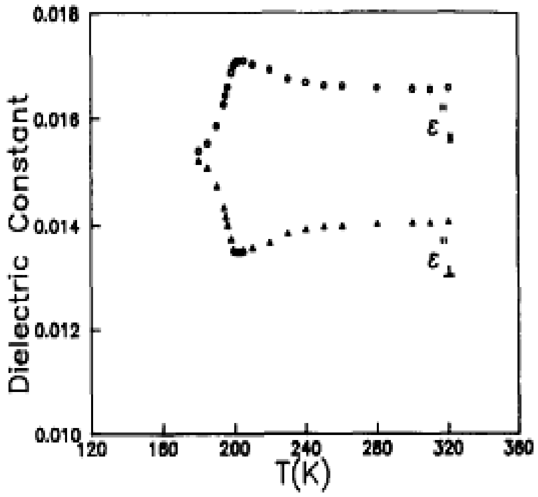

FIG. 42. Real parts $\varepsilon'_{\parallel}$ and $\varepsilon'_{\perp}$ of the dielectric constant versus temperature.

The results show that before a given temperature forking is not observed. Above such a temperature a separation between $\varepsilon_{\parallel}$ and $\varepsilon_{\perp}$ for both the real and imaginary parts is observed. Furthermore, the results show that both the real and imaginary parts of $\varepsilon_{\parallel}$ increase with temperature reaching a maximum at a given temperature then they both decrease for higher temperatures.

However, both the real and imaginary parts of $\varepsilon_{\perp}$ decrease with temperature reaching a minimum at a given temperature then both, increase for higher temperatures. The results also show that the temperature at which $\varepsilon_{\parallel}$ reaches it maximum is the same temperature at which $\varepsilon_{\perp}$ reaches its minimum. Thus the separation is enhanced by increasing the temperature till it reaches a maximum and by further increase of temperature the separation starts to decrease.

Furthermore, the results also show that at any temperature after the separation between $\varepsilon_{\parallel}$ and $\varepsilon_{\perp}$, the two differences ($\varepsilon_{\parallel}$ - ε_o) and (ε_o - $\varepsilon_{\perp}$) are equal and thus yield the value of 1 for the dielectric anisotropy factor g. This behavior of the dielectric anisotropy is explained in terms of the two competing effects, the orienting effect and the randomizing effect. At low temperature when the sample is in the frozen state, mechanical anisotropy does not exist in the sample resulting in the absence of the dielectric anisotropy. By increasing the temperature, particles are unblocked and are allowed to rotate and orient in the field direction. Therefore the average projection of these particles in the field direction becomes larger than in a direction normal to the field. Consequently, a sort of mechanical anisotropy is present in the sample leading to a difference between $\varepsilon_{||}$ and $\varepsilon_{\perp}$. Increasing the temperature further results in a higher rate of unblocking of particles contributing to the dielectric anisotropy. This process continues till the dielectric anisotropy reaches a maximum at a given temperature where the condition of alignment and chain formation in the field condition is optimum. For higher temperature the role of thermal agitation, *i.e.* randomizing effect becomes dominant leading to a reduction in the mechanical anisotropy and thus to a decrease in the dielectric anisotropy. Again it is the balance between these two competing effects that determines the behavior of the dielectric anisotropy in magnetic fluids.

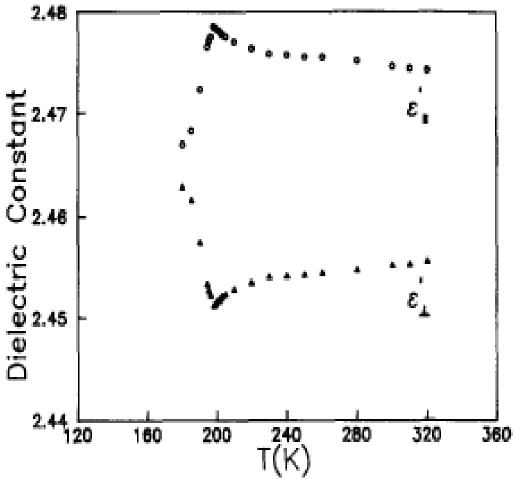

FIG. 43. Imaginary parts $\varepsilon''_{||}$ and $\varepsilon''_{\perp}$ of the dielectric constant versus temperature.

3.5- Wavelength Dependence of the Dielectric Anisotropy

Measurements of birefringence were undertaken using a quartz lamp, and narrow band interference filters. Similarly, dichroism was measured using the same light source and the wavelengths were also selected by narrow band interference filters.

The real part of the refractive index, n_o of the sample under zero fields (for all wavelength used) is determined by measuring the Brewster angle. Moreover, the extinction coefficient k_o of the samples (for all wavelengths) is determined by measuring the transmission of light through cells of different optical paths filled with the sample. The cells are standard cells made of the same glass having the same thickness.

The wavelength and concentration dependence of the real part of the index of refraction of the magnetic fluids, under zero fields, used are shown in Fig. 44 and Fig.45.

The wavelength and concentration dependence of the extinction coefficient, under zero fields, of the samples used are shown in Fig. 46 and Fig. 47.

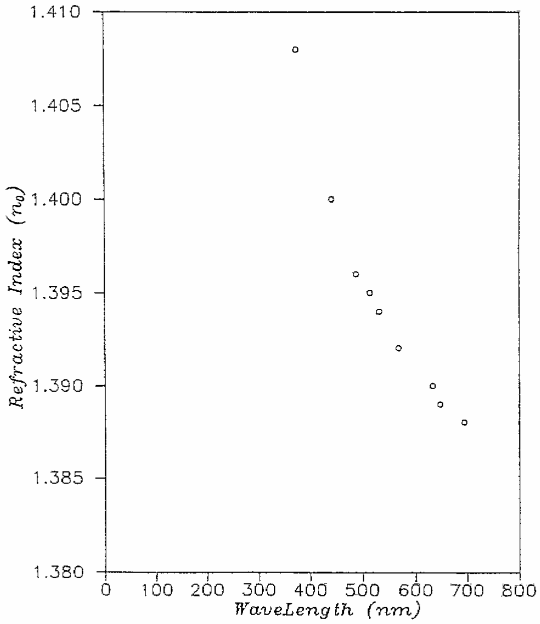

FIG. 44. Real index of refraction, n_o versus wavelength.

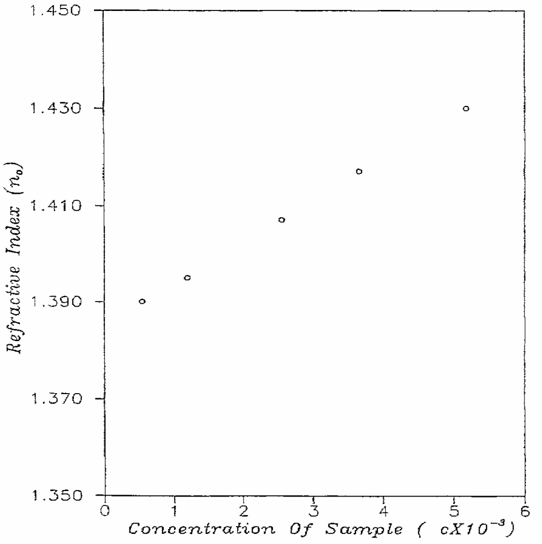

FIG. 45. Real index of refraction, n_o versus concentration

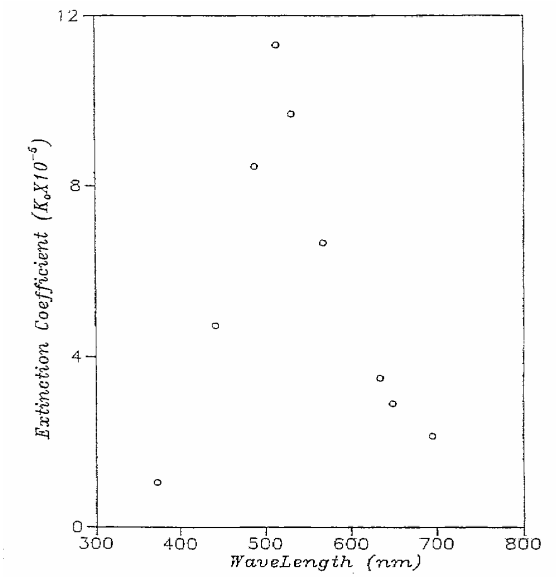

FIG. 46. Extinction coefficient, k_o versus wavelength

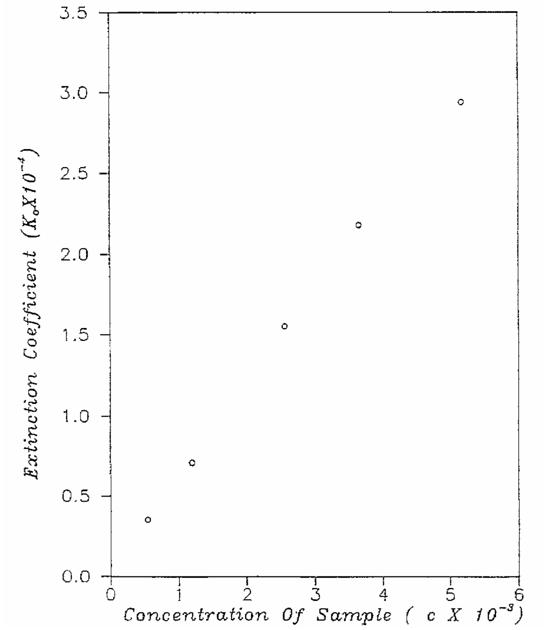

FIG. 47. Extinction coefficient, k_o versus concentration

The change in both the real and imaginary parts of the dielectric constant was calculated from birefringence, dichroism; the real part of the index of refraction at zero fields and the extinction coefficient of the samples at zero fields.

These calculations were undertaken for a three dimensional case. The results of the calculations, for the real part are presented in Fig. 48; while those for the imaginary part are presented in Fig. 49. The results in Fig. 48 show that the change in the real part of the parallel component, $\varepsilon_{\|}$, for all measuring fields, increases with wavelength reaching a maximum at a given wavelength then starts decreasing for longer wavelengths. Furthermore, the results also show that the change in the real part of the normal component, $\varepsilon_{\perp}$, for all measuring fields, decreases with wavelength reaching a minimum at a given wavelength then starts increasing for longer wavelengths.

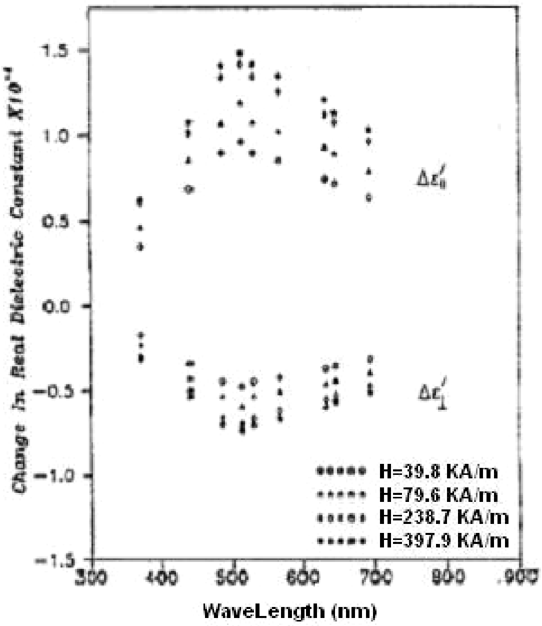

FIG. 48. Changes in the real parts, $\Delta\varepsilon'_{\|}$ and $\Delta\varepsilon'_{\perp}$ versus wavelength at different measuring fields.

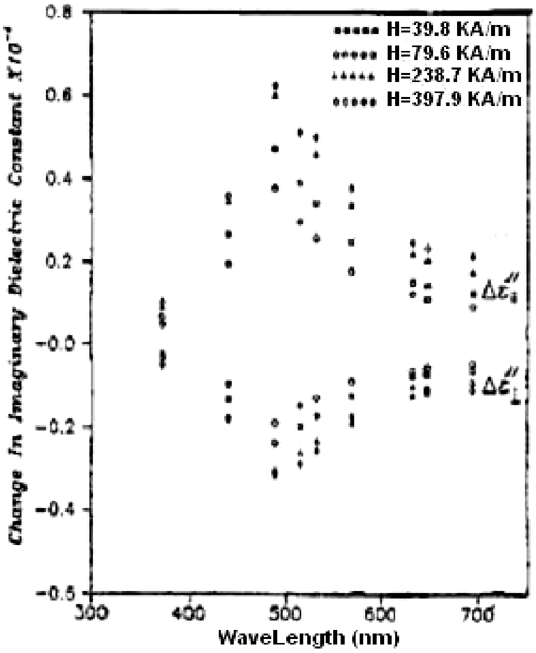

FIG. 49. Changes in the imaginary parts, $\Delta\varepsilon''_{\|}$ and $\Delta\varepsilon''_{\perp}$ versus wavelength at different measuring fields.

The results also show that the wavelength, at which the change in $\varepsilon_{\|}$ is a maximum, is the same wavelength at which the change in $\varepsilon_{\perp}$ is a minimum. This result is in agreement with the theory. For the imaginary part of the dielectric constant, the results show a similar behavior to that of the real part.

Comparing the results on the real and imaginary parts shows that, in agreement with the theory, the maximum change in the imaginary part occurs at a higher wavelength than the change in the real part; again, the results also show that the dielectric anisotropy factor g is 2.

The controversial value for the dielectric anisotropy factor, $g(H,\omega)$ has been resolved, it is shown that this factor takes the value of 1 for a two dimensional sample and the value of two for a three dimensional sample.

4- Numerical Calculations

4.1- Magneto-Optical Anisotropy

4.1.1- Method of Calculations

The optical anisotropy was numerically calculated for magnetic fluids with magnetic particles of different uniform sizes, flat-top size distribution, log-normal size distribution and normal size distribution; all the distributions have different mean values and standard deviations. For the normal distribution the calculations were carried out for different concentrations, different measuring fields and different liquid carriers.

The first step in the calculation carried out by Yusuf *et al* [80] is determining the Shliomis volume, V_S at a given temperature by numerically solving Eq. (20). Although Eq. (20) has two roots, the large root is taken as the accepted solution since the other root yields volumes (~ few Å in diameter) physically unacceptable because for these small radii the particles prefer the N$e'el$ relaxation mechanism. For particles with a uniform size, V the Shliomis volume at a given temperature V_S, is compared to the size of the particles, and if $V_S > V$, the optical anisotropy is put equal to zero. However if $V_S < V$, the parameter q is calculated and the integral $I(q)$ given in Eq. (29) is numerically evaluated and consequently the function $\xi(q)$ is evaluated. Moreover, for a given measuring field, H the parameter p is calculated at that given temperature and for the volume V, and consequently the function $f(p)$ given in Eq. (30) is evaluated. Therefore the orientation function $\Phi(p,q)$ is evaluated; and the optical anisotropy is then obtained by multiplying the orientation function by a constant which is proportional to the concentration. These calculations are repeated for different temperatures up to 350 K.

For a particle size distribution the Shliomis volume at a given temperature, V_S is compared to the distribution and if $V_S > V_{\max}$, where Vmax is the maximum volume in the distribution, the optical anisotropy is taken to be zero. However if $V_S < V_{\max}$, then particles with volumes $V_S < V < V_{\max}$ will contribute to the optical anisotropy at this given temperature. The range of volumes between V_S and $V_{\max}$ is divided into a number of narrow slices; and for each volume in this range the optical anisotropy is evaluated with the same procedure used in calculating the optical anisotropy for particles with uniform sizes. The total optical anisotropy at this temperature is then obtained by integrating numerically over the volume range from V_S to $V_{\max}$ when ($V_S > V_{\min}$), and from $V_{\min}$ to $V_{\max}$ when ($V_S < V_{\min}$). Here $V_{\min}$ is the minimum volume in the distribution. The number of slices used in this integration procedure was automatically set by using a divergence test. Changing the temperature will change the Shliomis volume and consequently the range of volumes for which particles will contribute to the optical anisotropy will change. Again the optical anisotropy is similarly calculated at different temperatures up to 350 K.

The effect of the applied magnetic field on the anisotropy energy, i.e., replacing KV by $KV[1 + (H/H_K)^2]$ where H_K is the anisotropy field $(M_{sB}/2K)$, has been introduced in the Néel relaxation time given in Eq. (18). This effect results in increasing the Néel relaxation time and consequently a lower Shliomis volume is obtained when solving Eq. (20).

The effect of concentration on the calculations of the optical anisotropy is introduced in the variation of viscosity with concentration, i.e., the relation in Eq. (21); and in the variation of viscosity with temperature Eqs. (22, 23) by slightly changing the value of T_o.

The effect of the liquid carrier on the optical anisotropy has been taken into consideration by choosing the proper values of the initial viscosity η_o and the melting point which in turn affects the value of T_o.

The values of the general constants used in the calculations are listed in Table 1.

TABLE 1. The values of the general constants used in the calculations

The effective anisotropy constant	$K = 5 \times 10^4$ J/m ^{3}
The attenuation factor	$\alpha = 1 \times 10^{-2}$
The gyromagnetic ratio	$\gamma = 1.7 \times 10^7$ S^{-1} G^{-1}
The saturation magnetization	$M_{sB} = 485$ kA/m
The constant A in Eq. (33)	$A = 396$ K
Re $(\breve{g}_a - \breve{g}_b)$	= 0.17

The birefringence Δn was calculated for single size magnetic particles dispersed in kerosene, with volumic fraction, ϕ equal to 0.05. Four different volumes of the particles were used (V = (6, 8, 10, 12, 14) × 10^{-25} m^3). The initial viscosity $\eta_o = 5.77 \times 10^{-3}$ Pa, and $T_o = 165$ K were used in the calculations.

A flat-top distribution with a mean volume $V_{mean} = 10 \times 10^{-25}$ m^3 and half width of 3×10^{-25} m^3 was also used in calculating the birefringence Δn for Fe_3O_4 particle magnetic fluid with kerosene as a liquid carrier and volumic fraction $\phi = 0.05$.

The same calculations were also carried out for the lognormal and normal distributions with the same mean volume used in the flat-top distribution. The standard deviation, σ, was taken 1×10^{-25} m^3 for the normal distribution and 0.15 for the log-normal distribution.

For normal distribution, the calculations were carried out for a given mean volume but with different standard deviations. They were also carried out for a given standard deviation but with different mean volumes.

The effect of the applied magnetic field on the optical anisotropy was investigated by using a normal size distribution with V_{mean} = 10×10^{-25} m^3 and with standard deviation, σ, equals 1×10^{-25} m^3. The applied magnetic field, H ranged from (8-160 kA/m). In the calculations the anisotropy energy KV is replaced by $KV\,[1 + (H/H_K)^2]$.

The effect of concentration on the optical anisotropy was investigated using the same normal size distribution used to study the effect of the applied magnetic field. The applied magnetic field is 39.8 kA/m. The change in viscosity due to the change in concentration is accounted for using the relation in Eq. (21). The parameter T_o entering the viscosity through Eqs. (22, 23) is changed slightly with concentration.

In Table 2 is a list of the volumic fraction of the particles in the magnetic fluid and the corresponding values of T_o.

TABLE 2. The volumic fraction ϕ and the melting points T_o for kerosene based magnetic fluids

ϕ	T_o (K)
0.025	164
0.050	166
0.075	168
0.100	170

The effect of the liquid carrier on the optical anisotropy is investigated using the same normal size distribution used in studying the effects of both concentration and applied magnetic field on the optical anisotropy. The volumic fraction, ϕ, is 0.05 and the applied field is 39.8 kA/m.

In Table 3 is a list of the different liquid carriers used and their corresponding initial viscosity η_o and the values of T_o.

TABLE 3. Different carriers and their corresponding initial viscosity and melting points

Liquid carrier	Initial viscosity η_o (P) × 10^{-3}	Melting point T_o (K)
Isopar-M	3.5	152
Kerosene	5.77	164
Toluene	9.2	169
Declain	20.0	175

4.1.2- Results of the Calculations

The birefringence Δn for a kerosene based magnetic fluid with ϕ = 0.05 and uniform particle sizes (V = (8, 10, 13) × 10^{-25} m^3) in a measuring field H = 39.8 kA/m is calculated. The results presented in Fig. 50 show that Δn is zero for T less than a given temperature T_S and that it suddenly jumps to a maximum value at a given temperature T_S.

The results also show that Δn decreases with temperature for $T > T_S$. Moreover, the results show that the larger the uniform size of the particles is, the lower the temperature T_S is and that it ranges from 186-219K. Furthermore, Δn is always zero for $V < 6 \times 10^{-25}$ m^3 in this range of temperatures. This behavior is a result of the variation of the Shliomis volume with temperature [80-81]. Because the optical anisotropy is a consequence of the mechanical anisotropy the birefringence Δn will not be observed before $V_S \leq V$. Once a temperature T_S at which $V_S \leq V$ is reached all the particles in the fluid will contribute to the optical anisotropy in unison and therefore a sudden jump in birefringence takes place. For temperatures $T > T_S$ thermal agitation is the dominant factor and Δn decreases with temperature in this range. Moreover, for small sizes, V_S is always greater than these volumes and the particles relax via the N$e'el$ relaxation mechanism leading to no birefringence.

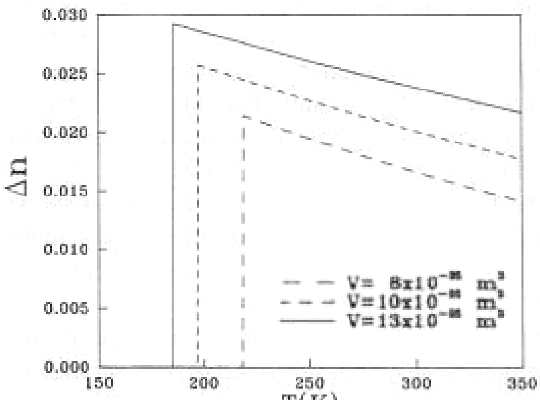

FIG. 50. Birefringence, Δn versus temperature for different uniform sizes.

The birefringence Δn is calculated for a kerosene based magnetic fluid with ϕ = 0.05 and a measuring field H = 38.9 kA/m for different size distributions. These are the flat-top, the log-normal and the normal distributions. In all three distributions the mean volume is the same (V_{mean} = 10 × 10^{-25} m^3) and both $V_{\max}$ and $V_{\min}$ are reasonably the same.

The results of these calculations presented in Fig. 51 show that the basic features of birefringence are practically not changed by changing the type of distribution. Furthermore, the results show that the magnetic fluid shows no birefringence (optical anisotropy) below a temperature T_S ranging from 182 to 185 K and that it exhibits a degree of optical anisotropy for $T > T_S$. The results also show that the optical anisotropy increases rapidly (but not suddenly) with temperature reaching a maximum at a temperature T_m = 219, 226 and 240 K for the normal, log-normal and the flat-top distributions, respectively, then it decreases with temperature. This behavior of the optical anisotropy with temperature is similar to that found experimentally [18-20, 41].

For a particle size distribution there are particles with volumes larger than the mean volume of the distribution; consequently the temperature at which Δn appears for a distribution is expected to be lower than that for a uniform size. Furthermore, not all the particles will concurrently contribute to the optical anisotropy but rather gradually depending on their volumes. Therefore, the rise of Δn to its maximum value is rapid but not sudden. It is clear that the type of distribution does not affect the general basic features of Δn and as a result only the normal distribution will be used.

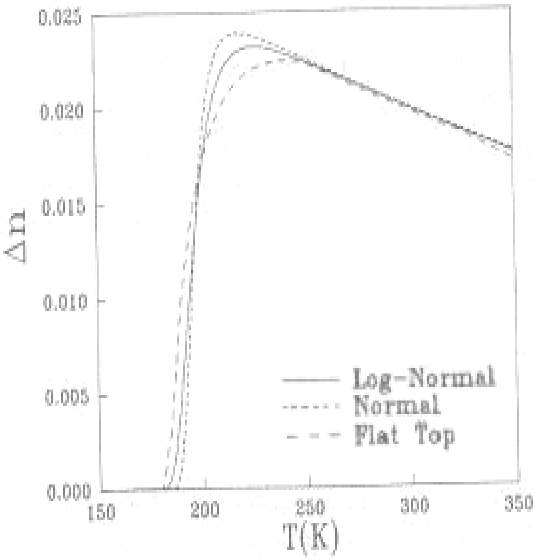

FIG. 51. Birefringence, Δn versus temperature for different size distributions.

The birefringence, Δn is calculated for kerosene based magnetic fluid using a normal size distribution of the particles with three different mean volumes ((10, 12, 14) × 10^{-25} m^3) and one standard deviation $\sigma = 1 \times 10^{-25}$ m^3. The results of the calculations are presented in Fig. 52.

The results in the figure show that the larger the mean volume is, the lower both T_S and T_m are. Furthermore, they also show that the larger the mean volume is, the steeper the rise of Δn from zero to its maximum value is. A sample with a large mean volume has a larger portion of particles with volumes greater or equal to the Shliomis volume, just after the slurry state, than a sample with smaller mean size. Consequently, more particles contribute to the optical anisotropy and hence the rise from zero anisotropy to its maximum value is steeper. Again this behavior is consistent with the variation of V_S with temperature and its relation to the volumes of the particles.

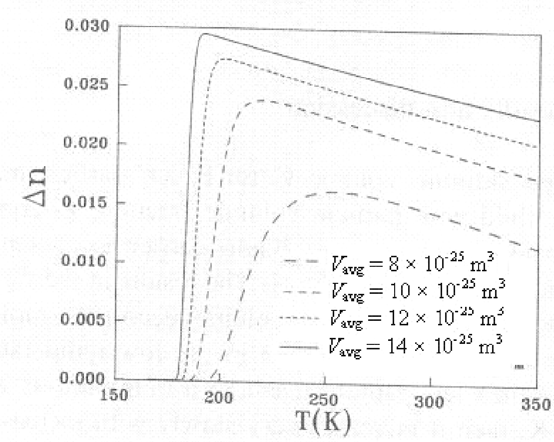

FIG. 52. Birefringence, Δn calculated for a normal size distribution of different mean volumes but the same standard deviation.

The effect of the standard deviation, σ, on Δn is also investigated by calculating the optical anisotropy using normal distributions with the same mean volume but with different standard deviations. The results show that for a given mean volume, the larger σ is, the lower T_S is. Furthermore, they also show that the larger σ is the broader the peak is. Having a large σ increases $V_{\max}$ and lowers $V_{\min}$, *i. e*, widens the range of the distribution, and therefore the temperature T_S at which birefringence, Δn, appears is lowered. The peak is broader due to the more gradual conversion of blocked particles, ($V < V_S$), to unblocked ones, ($V \geq V_S$), which now continues over a wider range of temperatures due to the widening of the distribution..

The birefringence Δn for kerosene based magnetic fluid with $\phi = 0.05$ and a normal particle size distribution ($V_{mean} = 10 \times 10^{-25}$ m^3, $\sigma = 1 \times 10^{-25}$ m^3) was calculated, for applied magnetic fields H ranging from 39-400 kA/m. The results of these calculations are shown in Fig. 53.

The results in the figure show, as expected, that the higher the measuring field is, the higher Δn is. More importantly the results also show that increasing the measuring field lowers both T_S and T_m. This behavior is similar to that observed experimentally [18, 41].

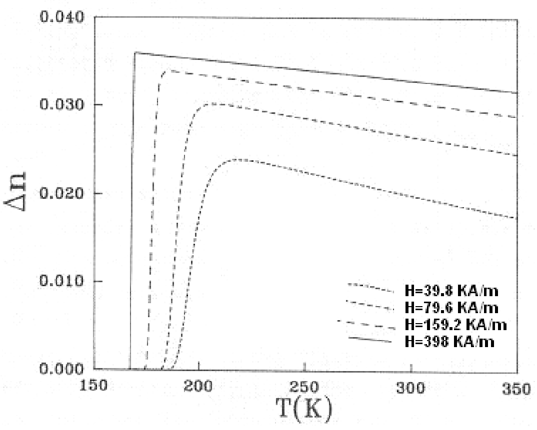

FIG. 53. Birefringence, Δn calculated for a normal size distribution for different applied fields.

Increasing the applied magnetic field has two effects, the first is to increase the anisotropy energy leading to an increase in τ_N and thus making the Brownian relaxation mechanism more favorable, and the equality between the two relaxation times can be reached at higher viscosities, *i.e.,* at lower temperatures.

The second effect is to increase the magnetic torque exerted on the particles which now overcomes a larger viscous torque, as a result the particles start to rotate and align in the field direction at lower temperature. Because the onset of the unblocking of particles occurs at a lower temperature, the maximum in alignment is achieved at lower temperatures for higher applied magnetic fields. Therefore, the temperatures at which the onset of birefringence occurs and at which the maximum is reached, are lower for higher applied fields.

The birefringence, Δn is calculated for kerosene based samples having the same normal size distribution, (V_{mean} = 10 × 10^{-25} m^3, σ = 1 × 10^{-25} m^3) but with different concentration using the same applied magnetic field, H = 39.8 kA/m. The results presented in Fig. 54 show, as expected, that increasing the concentration increases Δn. More importantly they also show that increasing the concentration increases both T_S and T_m.

The values of T_S ranges from 184 K for ϕ = 0.025 to 190 K for ϕ = 0.1 while T_m ranges from 216 K to 225 K. This behavior is similar to that observed experimentally [18, 41].

Increasing the concentration increases the viscosity of the sample and also its melting point leading to an increase in the Brownian relaxation time and thus the temperature at which $\tau_N = \tau_B$ is increased. Consequently the onset of birefringence occurs at higher temperatures for higher concentrations, and also the temperature at which the maximum in birefringence occurs is higher for higher concentrations.

The birefringence Δn is calculated for magnetic fluids of the same concentration but with different liquid carriers. Normal particle size distribution (V_{mean} = 10 × 10^{-25} m^3, σ = 1 × 10^{-25} m^3) and a measuring magnetic field (H = 39.8 kA/m) are used in these calculations. The liquid carriers used and their corresponding initial viscosities and melting points are listed in Table3. The results of these calculations are shown in Fig. 55.

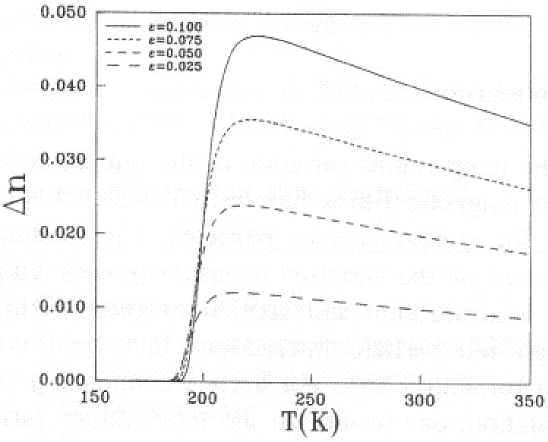

FIG. 54. Birefringence, Δn calculated for a normal size distribution for different concentration and an applied field 38.9 kA/m.

The results in the figure show that the lower both the viscosity and the melting point of the carrier are, the lower both T_S and T_m are. The value of T_S ranges from 170 K for Isopar-M (Lowest initial viscosity) based magnetic fluid to 206 K for Declain (highest initial viscosity) based magnetic fluid; while T_m ranges from 196 K to 258 K respectively. Furthermore, they also show that the lower η_o and T_o are the higher the birefringence at a given temperature is. This behavior is similar to that observed experimentally [19].

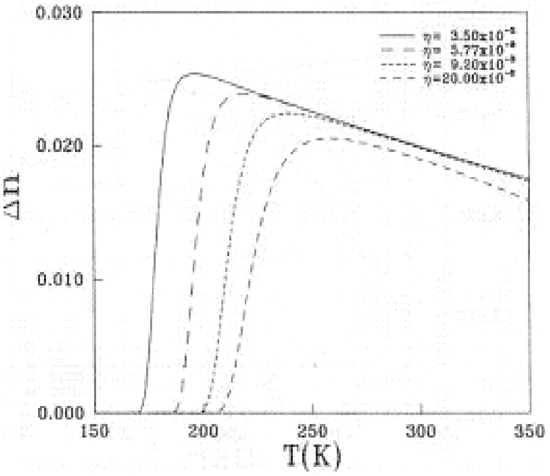

FIG. 55. Birefringence, Δn calculated for a normal size distribution for magnetic fluids with different liquid carriers

Lowering the initial viscosity of the sample reduces the Brownian relaxation time at all temperatures and hence allows more particles to contribute to the optical anisotropy at lower temperatures.

Furthermore, it also reduces the viscous torque thus making the magnetic torque capable to rotate the particles in the field direction. Hence, the temperature at which the onset of the optical anisotropy occurs is lowered. Decreasing the melting point of the carrier lowers the temperature at which the slurry state is reached. Also result both T_S and T_m are lowered by lowering the initial viscosity and melting point of the liquid carrier.

For a low viscosity sample, a larger portion of the particles, in comparison to high viscosity sample, become unblocked at low temperature when the thermal agitation is not yet very effective in randomizing the particles, therefore, the optical anisotropy for low viscosity samples is larger than that for high viscosity samples.

Based on the orientation of the particles in the magnetic field direction, that produces two different average projection lengths one is parallel to the field and the other is normal, the magneto-optical anisotropy was calculated. It is found that taken into consideration the completion between the N$e'el$ relaxation and the Brownian relaxation and the role of temperature in randomizing the already aligned particles, on the one hand, and of changing the viscosity on the other hand, is sufficient to produce all the basic features of the optical anisotropy that were observed experimentally. Therefore, it is concluded that the orientation of the particles and the chain formation in the fluid is the main cause of the magneto-optical anisotropy effects in magnetic fluids.

4.2- Magneto Dielectric Anisotropy Effect

4.2.1- Method of Calculations

The magneto-dielectric anisotropy effect in magnetic fluids was calculated numerically by Yusuf and co-workers [81] for two and three-dimensional magnetic fluid samples. The assumption is that the dielectric constant at a given wavelength is proportional to the average projection length of the particles in the fluid. Based on this assumption, they have calculated the dielectric constant, $\varepsilon_{\parallel}$ for electromagnetic waves polarized in the field direction, and, $\varepsilon_{\perp}$ for electromagnetic waves polarized normal to the field direction.

For an ellipsoidal particle with a major axis a and a minor axis b, the average projection lengths $l_{\parallel}$, parallel to the field and, $l_{\perp}$ perpendicular to the field, for a two dimensional system are expressed as:

$$l_{\parallel} = a[1+\Phi(p,q)] + \frac{b}{2}[1-\Phi(p,q)] \tag{70}$$

and

$$l_{\perp} = a[1-\Phi(p,q)\} + \frac{b}{2}[1+\Phi(p,q)] \tag{71}$$

where $\Phi(p,q)$ is the orientation function given by Eq.27.

These two equations ensure the boundary condition that the average values of $l_{\parallel}$, and, $l_{\perp}$, are the same and equal to $(\frac{2a+b}{2})$ at zero field where $\Phi(p,q)$ = 0; and those at very high fields where $\Phi(p,q)$ = 1 are, $l_{\parallel}$ = $2a$ and, $l_{\perp} = b$.

For a three-dimensional system with a field applied in the z direction the average projection lengths are expressed as:

$$l_{\|} = \frac{2a}{3}(1 + 2\Phi(p,q)) + \frac{2b}{3}(1 - \Phi(p,q)) \quad (72)$$

and

$$l_{\perp} = \frac{2a}{3}(1 - \Phi(p,q)) + \frac{2b}{3}(1 + \Phi(p,q)) \quad (73)$$

Again the last two equations ensure the boundary conditions that $l_{\|}$, and, $l_{\perp}$, are the same and equal to $(\frac{2(a+b)}{3})$ at zero field where $\Phi(p,q) = 0$; and that $l_{\|} = 2a$ and, $l_{\perp} = b$ at very high fields where $\Phi(p,q) = 1$

Taking into consideration the particle size distribution, the total average projection lengths, for a 2D system will be given by:

$$\left.\begin{aligned} l_{\|T} = &\int_{V_{\min}}^{V_s} (\frac{2a+b}{2})F(V)dV + \\ &\int_{V_S}^{V_{\max}} \{a[1 + \Phi(p,q)] \\ &\qquad + \frac{b}{2}[1 - \Phi(p,q)]\}F(V)dV \end{aligned}\right\} \quad (74)$$

and

$$\left.\begin{aligned} l_{\perp T} = &\int_{V_{\min}}^{V_S} (\frac{2a+b}{2})F(V)dV + \\ &\int_{V_S}^{V_{\max}} \{a[1 - \Phi(p,q)] \\ &\qquad + \frac{b}{2}[1 + \Phi(p,q)]\}F(V)dv \end{aligned}\right\} \quad (75)$$

However, for a three-dimensional system, the projection lengths are given by:

$$\left.\begin{aligned} l_{\|T} = &\int_{V_{\min}}^{V_S} (\frac{2(a+b)}{3})F(V)dV + \\ &\int_{V_S}^{V_{\max}} \{\frac{2a}{3}(1 + 2\Phi(p,q)) \\ &\qquad + \frac{2b}{3}(1 - \Phi(p,q))\}F(V)dV \end{aligned}\right\} \quad (76)$$

and

$$\left.\begin{aligned} l_{\perp T} = &\int_{V_{\min}}^{V_S} (\frac{2(a+b)}{3})F(V)dV + \\ &\int_{V_S}^{V_{\max}} \{\frac{2a}{3}(1 - \Phi(p,q)) \\ &\qquad + \frac{2b}{3}(1 + \frac{\Phi(p,q)}{2})\}\, F(V)\, dV \end{aligned}\right\} \quad (77)$$

Where $V_{\min}$ and $V_{\max}$ are the minimum and maximum volumes in the distribution, respectively, and V_S is the Shliomis volume.

The total average lengths $l_{\|T}$, and, $l_{\perp T}$ were calculated for magnetic fluids with magnetic particles of different uniform sizes, log-normal, and normal size distributions. The first step in the calculation is determining the Shliomis volume V_S at a given temperature and for a given applied field by numerically solving Eq. 20. For particles with a uniform size V, the Shliomis volume, V_S, at a given temperature and for a given applied field is compared to the size of the particles, and if $V_S > V$ both $l_{\|T}$, and, $l_{\perp T}$, are set equal to $(\frac{2a+b}{2})$ for a two-dimensional sample, $\frac{2(a+b)}{3}$ for a three-dimensional sample. However if $V_S < V$, the parameter q is calculated and the integral $I(q)$ given in Eq. 29 is numerically evaluated, and consequently the function $\xi(q)$ is evaluated. Moreover, for a given measuring field H and a given temperature, the parameter p is calculated for the volume V, and consequently the function $f(p)$ given in Eq. 30 is evaluated. Therefore, the orientation function $\Phi(p,q)$ is evaluated, and the average projection lengths, $l_{\|}$ and

$l_{\perp T}$, are then obtained from Eqs.74 and 75, for the two-dimensional system, and from Eqs.76 and 77, for the three-dimensional system. By multiplying the average projection lengths by a constant (for a given wavelength), which is proportional to the concentration, the relative dielectric constant is obtained. Dividing these quantities by their corresponding values at zero fields (ε_o which is equal to $(\frac{2a+b}{2})$ multiplied by the same constant for 2-D sample and $\frac{2(a+b)}{3}$ multiplied by the same constant for 3-D sample), yields ($\varepsilon_{\|} \ / \ \varepsilon_o$) and ($\varepsilon_{\perp} \ / \ \varepsilon_o$). These calculations are repeated for different temperatures and different applied magnetic fields for different single volumes. The axial ratio (a/b) used in these calculations ranged from 1.0 to 2.0.

For a particle size distribution the Shliomis volume at a given temperature and at a given applied field V_S is compared to the distribution and if $V_S > V_{\max}$ then the average lengths $l_{\|T}$, and, $l_{\perp T}$, are taken equal to that when the applied field is zero l_o, where l_0 is given by:

$$l_o = \int_{V_{\min}}^{V_{\max}} (\frac{2a+b}{2}) F(V) dV \qquad (78)$$

for the two-dimensional samples and

$$l_o = \int_{V_{\min}}^{V_{\max}} \frac{2(a+b)}{3} F(V) dV \qquad (79)$$

for the three-dimensional samples.

However if $V_S < V_{\max}$, then particles with volumes $V_S \leq V \leq V_{\max}$ will orient with the field and the values $l_{\|}$, and, $l_{\perp}$, are given by Eqs.70 and 71 for the 2-D system, and Eqs.72 and 73 for the 3-D system. The range of volumes between $V_{\min}$ and $V_{\max}$ is divided into a number of narrow slices, and for each volume in this range the values $l_{\|}$ and, $l_{\perp}$, are evaluated with the same procedure used in the case of particles with uniform sizes. The total average lengths at a given temperature and a given applied field is then obtained by numerically integrating over the volume range from $V_{\min}$ to $V_{\max}$ using Eqs. 74 and 75 for the 2-D system and Eqs. 76 and 77 for the 3-D system. Changing the temperature or the applied field will change the Shliomis volume and consequently the range of volumes for which particles will orient with the field will change. The relative dielectric constants ($\varepsilon_{\|} \ / \ \varepsilon_o$) and ($\varepsilon_{\perp} \ / \ \varepsilon_o$) are then calculated from ($\varepsilon_{\|} \ / \ \varepsilon_o = l_{\|} \ / \ l_o$) and ($\varepsilon_{\perp} \ / \ \varepsilon_o = l_{\perp} \ / \ l_o$).

The effect of the applied magnetic field on the anisotropy energy, i.e., replacing KV by $KV[1 + (H/H_K)^2]$ where H_K is the anisotropy field ($M_{sb}/2K$), has been introduced in the Néel relaxation time given in Eq. (18). This effect results in increasing the Néel relaxation time and consequently a lower Shliomis volume is obtained when solving Eq. (20).

The effect of concentration on the calculation is introduced in the variation of viscosity with concentration, i.e., the relation in Eq. (21); and in the variation of viscosity with temperature Eqs. (22), and (23) by slightly changing the value of T_o.

The effect of the liquid carrier on the optical anisotropy has been taken into consideration by choosing the proper values of the initial viscosity η_o and the melting point which in turn affects the value of T_o. The values of the general constants used in the calculations are listed in Table 1.

The reduced dielectric constant was calculated for uniform size Fe_3O_4 magnetic particles dispersed in kerosene, with volumic fraction ε equal to 0.05. Four different volumes of the particles were used (V = 6, 8, 10, 12, 14 × 10^{-25} m^3). The initial viscosity η_o = 5.77 × 10^{-3} Pa, and T_o = 165 K were used in the calculations. Furthermore, the reduced dielectric constant for Fe_3O_4 particle magnetic fluid with kerosene as a liquid carrier and volumic fraction ϕ =0.05 was calculated for normal and lognormal distributions with particle average volume of 8 × 10^{-25} m^3, and a standard deviation of 1 × 10^{-25} m^3 and 0.15, respectively. The effect of the liquid carrier on the magneto-dielectric effect is investigated by changing the initial viscosity and changing the parameter T_0.

4.2.2- Results of the Calculations

The magneto-dielectric anisotropy effect for uniform size (V = 8 × 10^{-25} m^3) Fe_3O_4 particle magnetic fluid (different axial ratios) with kerosene as a liquid carrier at a temperature T = 300 K versus magnetic field is presented in Figs. 56 and 57 for the 2-D and 3-D systems, respectively.

The results in the figures show that both ($\varepsilon_{||}$ / ε_o) and ($\varepsilon_\perp$ / ε_o) starts practically from 1.0 at very low fields and that ($\varepsilon_{||}$ / ε_o) increases rapidly for intermediate fields and tends to saturate at high fields; while ($\varepsilon_\perp$ / ε_o) decreases rapidly for intermediate fields and levels off at high fields. The rate of increase for ($\varepsilon_{||}$ / ε_o) and the rate of decrease for ($\varepsilon_\perp$ / ε_o) are dependent on the axial ratio (*a*/*b*) being the highest for the highest axial ratio. Furthermore, the highest value of ($\varepsilon_{||}$ / ε_o) and the lowest value of ($\varepsilon_\perp$ / ε_o) occurs for the highest axial ratio.

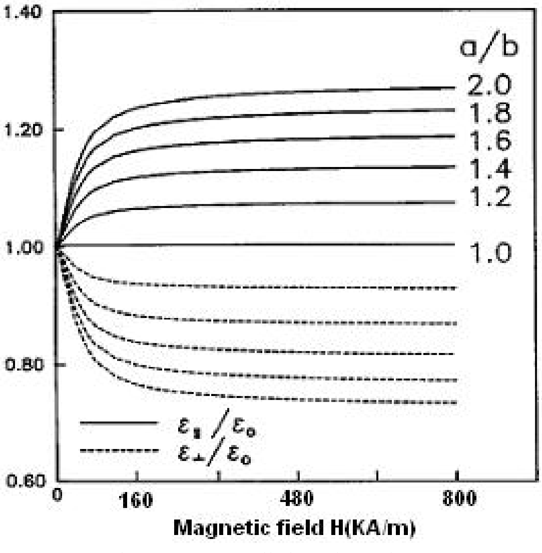

FIG. 56. The magneto-dielectric anisotropy effect for particles with single volume V = 8 × 10^{-25} m^3 and different axial ratios versus magnetic field (2-D case).

The results also show that for an axial ratio of 1.0, i.e., spherical particles, the magneto-dielectric effect is absent. The results also show that $g(H,\omega)$ = 1 for the 2-D system and 2 for the 3-D system. At T = 300 K, all the particles are unblocked and contribute to the mechanical anisotropy and hence to the dielectric anisotropy provided that some degree of orientation is present. Of course, at zero or very low fields the orientation function is zero resulting in equal average projection lengths $l_{||}$, and $l_\perp$, consequently the dielectric anisotropy is not observed. When the field becomes appreciable, and the orientation of the particles starts, a difference in the projection lengths $l_{||}$ and $l_\perp$ occurs resulting in the appearance of the dielectric anisotropy effect. At any given applied magnetic field, the higher the axial ratio is, the higher is the difference between $l_{||}$, and $l_\perp$, and consequently the higher is the dielectric anisotropy and also the steeper is the rise in it. For spherical particles, when chain formation is not taken into consideration, the two average lengths $l_{||}$ and $l_\perp$ are equal no matter what the applied field is and as a result the dielectric anisotropy is always zero. To allow for introducing the chain formation inter-particle interactions should be taken into consideration by studying the dynamics of the particles inside the fluid. Probably changing the axial ratio of the particle is some how equivalent to the formation of chains in the sample. It should be noted that a high axial ratio resembles a long chain.

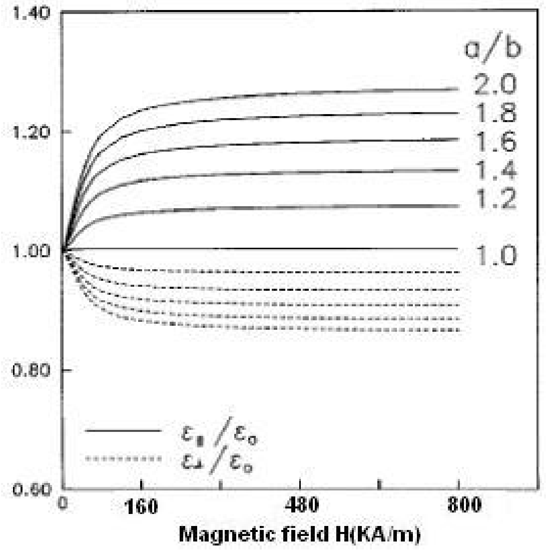

FIG. 57. The magneto-dielectric anisotropy effect for particles with single volume V = 8 × 10^{-25} m^3 and different axial ratios versus magnetic field (3-D case).

The effect of increasing the volume of the particles or the mean volume in a distribution is to increase the absolute difference between the two axes. This in turn increases the difference between $l_{\|}$ and $l_{\perp}$, leading to an increase in the dielectric anisotropy. Such a behavior is obtained by calculating the dielectric anisotropy for samples of the same concentration with normal particle size distribution of the same standard deviation but with different mean volumes. The results of calculations for normal size distribution with average volumes of 6, 8, 10, 12, and 14 × 10^{-25} m^3, axial ratio (a/b) = 1.2 and a standard deviation $\sigma = 1 \times 10^{-25}$ m^3 are presented in Figs. 58 and 59 for the 2-D and 3-D cases, respectively.

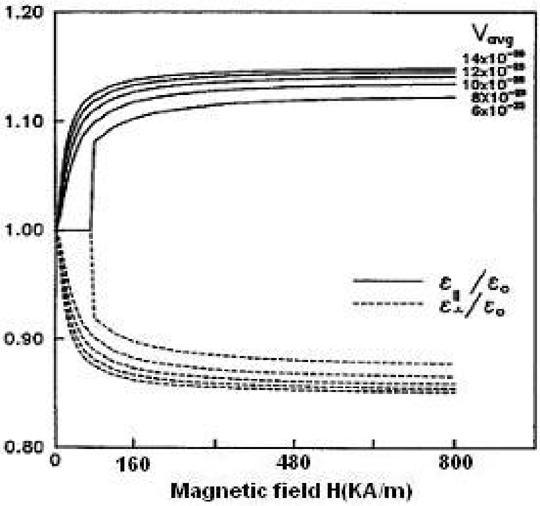

FIG. 58. The magneto-dielectric anisotropy effect for particles with the same axial ratio and standard deviation but different mean volumes plotted versus magnetic field (2-D case).

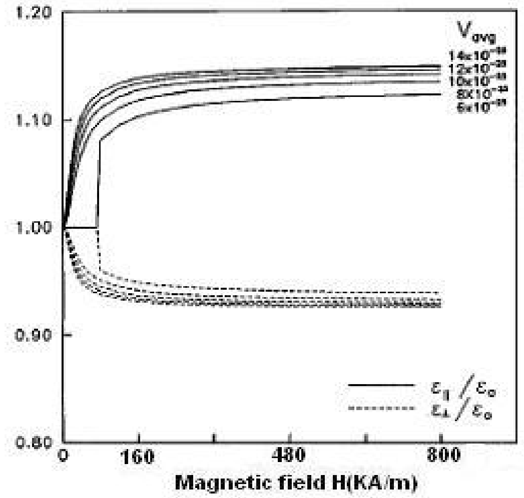

FIG. 59. The magneto-dielectric anisotropy effect for particles with the same axial ratio and standard deviation but different mean volumes plotted versus magnetic field (3-D case).

The results in the figures show that the higher the average volume is, the higher the magneto-dielectric anisotropy effect is. Also the results in the figures show that when the average volume is small the magneto-dielectric anisotropy effect does not appear until the field is appreciable. Furthermore, again the results show that $g(H,\omega)$ = 1 for the 2-D sample and 2 for the 3-D sample.

The magneto-dielectric anisotropy effect for a magnetic fluid with ϕ = 0.05 at temperature T = 300 K for single volume, normal distribution and log-normal distribution are presented in Figs. 60 and 61 for the 2-D and 3-D cases, respectively.

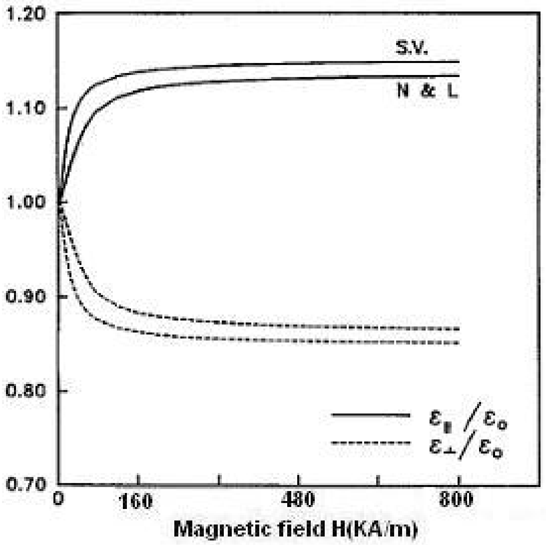

FIG. 60. The magneto-dielectric anisotropy effect for particles with single size, normal and log-normal distribution plotted versus applied field (2-D case).

For both cases the average volume for the two distributions is taken equal to the single volume ($V = 8 \times 10^{-25}$ m^3) but the standard deviation is taken 1×10^{-25} and 0.15 m^3, for the normal and log-normal distributions, respectively. For the three size distributions the axial ratio is 1.2. The results show that the magneto-dielectric anisotropy effect is the same for the two distributions and is slightly different for the single volume case.

However, although increasing the axial ratio leaves the similarity between the two distributions unchanged, the difference between them and the single volume case is further reduced. Again the results show that $g(H,\omega)$ = 1 for the 2-D sample and 2 for the 3-D sample.

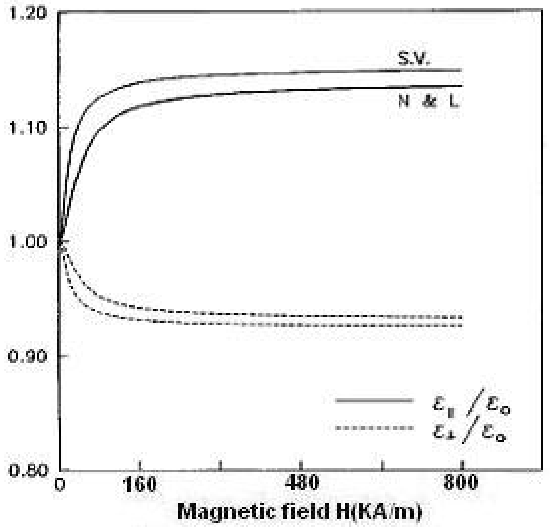

FIG. 61. The magneto-dielectric anisotropy effect for particles with single size, normal and log-normal distribution plotted versus applied field (3-D case).

The magneto-dielectric anisotropy effect versus temperature in a magnetic fluid with uniform, normal, and log- normal size distributions, measured at H = 39.8 kA/m is presented in Figs. 62 and 63 for the 2-D and 3-D cases respectively. The average volume for both distributions is equal to the single volume $V = 8 \times 10^{-25}$ m^3 and the axial ratio for the three cases is 1.6. The standard deviation is 1×10^{-25} and 0.15 m^3 for the normal and log-normal distributions, respectively.

The results show that the magneto-dielectric anisotropy effect is absent below a given temperature, T_S and that this temperature is different for the different size distributions, being the lowest for the normal distribution.

Above such a temperature, "forking" between $(\varepsilon_{\parallel} / \varepsilon_o)$ and $(\varepsilon_{\perp} / \varepsilon_o)$ starts, the parallel component increases while the normal component decreases till the first reaches a maximum while the second reaches a minimum at a temperature T_m. Beyond this temperature the parallel component starts to decrease with temperature while the normal component increase with temperature.

Furthermore the results also show that the increase to the maximum of $(\varepsilon_{\parallel} / \varepsilon_o)$ and the decrease to the minimum of $(\varepsilon_{\perp} / \varepsilon_o)$ is gradual in the case of the size distributions, while it is abrupt in the case of the single size.

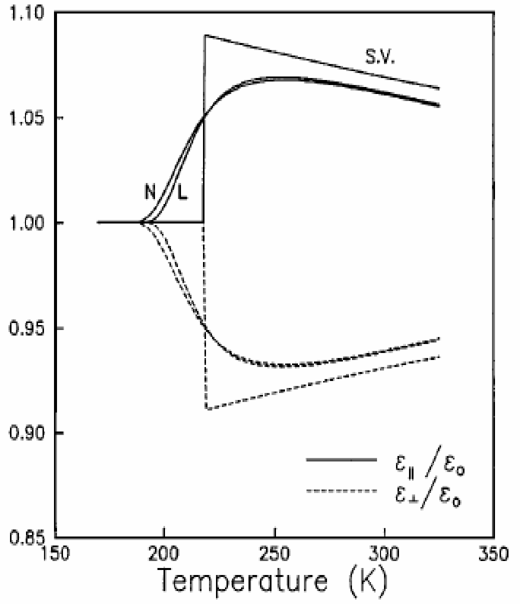

FIG. 62. The magneto-dielectric anisotropy plotted versus temperature for single, normal, and log-normal distributions (2-D case).

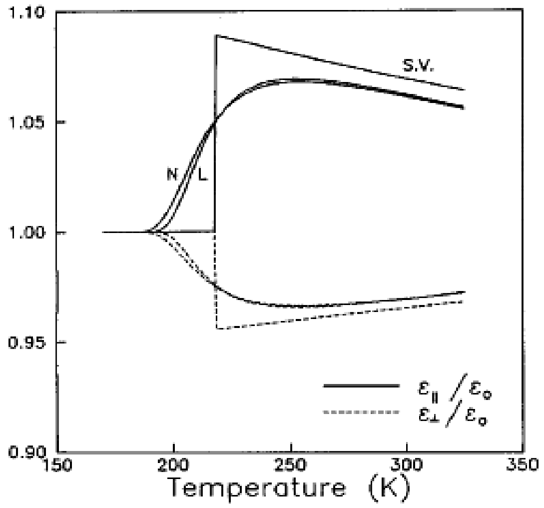

FIG. 63. The magneto-dielectric anisotropy plotted versus temperature for single, normal, and log-normal distributions (3-D case).

The results also show that the magneto-dielectric anisotropy effect for the normal or a log-normal size distribution are practically imposed but still deviate from that for a single volume. This behavior with temperature is explained in terms of the unblocking of particles allowing them to orient physically through the Brownian relaxation mechanism and also in terms of the two competing effects, the orienting effect due to the field and the randomizing effect due to thermal agitation. Again the results in the figure show that $g(H,\omega)$ = 1 for the 2-D sample and 2 for the 3-D sample. Increasing the temperature to a high enough value where the randomizing effect is highly dominant resulted in ($\varepsilon_{\|}$ / ε_o) and ($\varepsilon_{\perp}$ / ε_o) converging towards each other as is seen in Figs. 64 and 65.

It is important to note that the temperature at which this convergence starts can not be used experimentally because it is above the boiling point of the liquid carrier.

The magneto-dielectric anisotropy effect for a magnetic fluid, (ϕ = 0.05) with normal size distributions of an average volume of 8×10^{-25} m^3 and standard deviation of 1×10^{-25} m^3 and an axial ratio of 1.2 at different applied magnetic fields versus temperature is presented in Figs. 66 and 67 for the 2-D and 3-D cases, respectively.

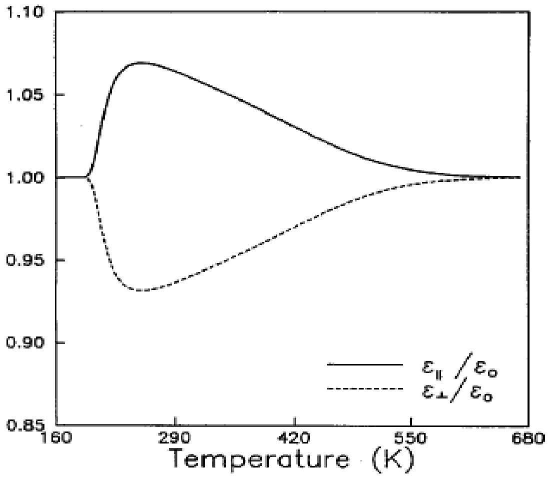

FIG. 64. The magneto-dielectric anisotropy plotted versus temperature (2-D case).

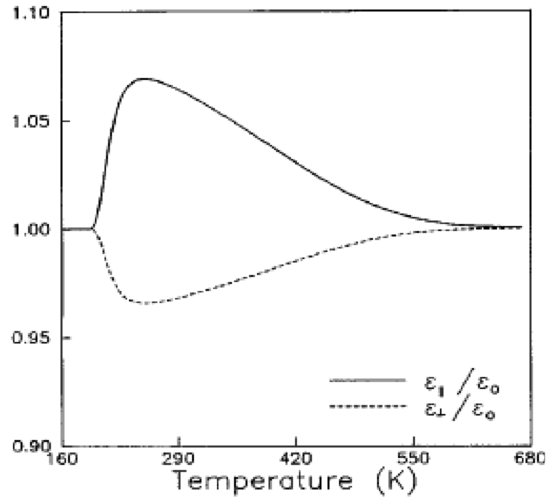

FIG. 65. The magneto-dielectric anisotropy plotted versus temperature (3-D case).

The results show that the general behavior of the magneto-dielectric anisotropy effect with temperature for different measuring fields is the same and is similar to that described above. However, the temperatures at which the magneto- dielectric anisotropy effect appears and at which it reaches an optimum are field dependent being the lowest for the highest field; and the dielectric effect is higher for higher fields. Increasing the applied magnetic field has two effects, the first is to increase the anisotropy energy leading to an increase in τ_N and thus making the Brownian relaxation mechanism more favorable, and the equality between the two relaxation times can be reached at higher viscosities, *i.e.,* at lower temperatures.

The second effect is to increase the magnetic torque exerted on the particles which now overcomes a larger viscous torque, as a result the particles start to rotate and align in the field direction at lower temperature. Because the onset of the unblocking of particles occurs at a lower temperature, the maximum in alignment is achieved at lower temperatures for higher applied magnetic fields. Therefore, the temperatures at which the onset of the dielectric anisotropy occurs and at which the maximum is reached, are lower for higher measuring fields.

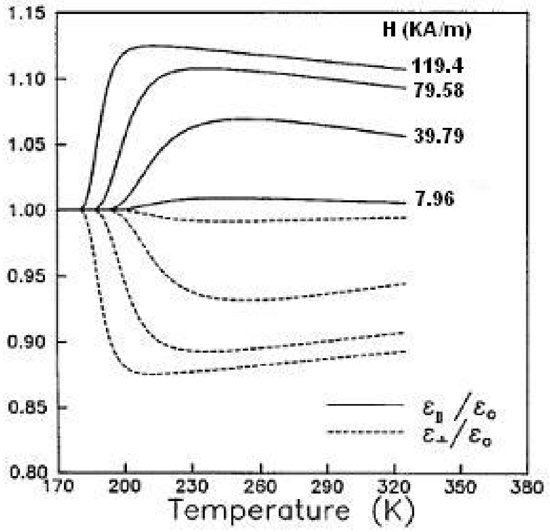

FIG. 66. The magneto-dielectric anisotropy plotted versus temperature for different measuring fields, (2-D case).

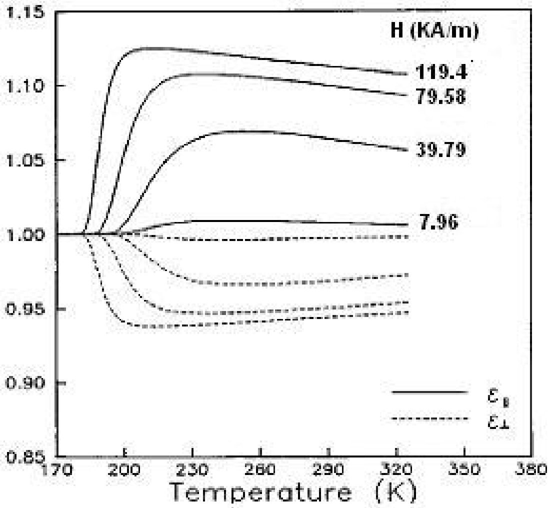

FIG. 67. The magneto-dielectric anisotropy plotted versus temperature for different measuring fields, (3-D case).

Furthermore, the results show that changing the axial ratio of the particles while keeping all other parameters the same, changes only the magnitude of the effect, but does not change the temperature at which the effect appears nor at which it is a maximum, as can be seen in Fig. 68.

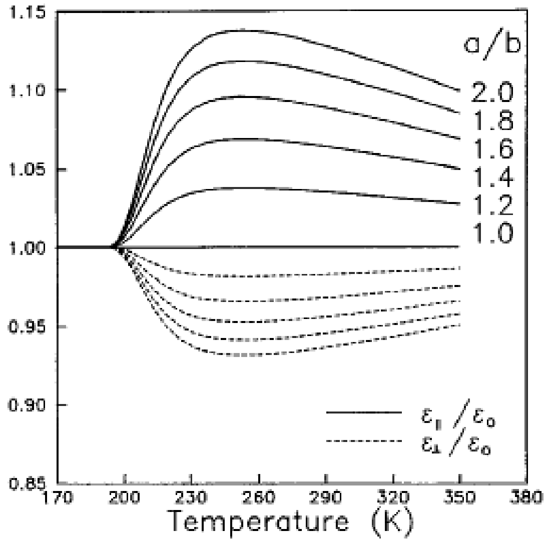

FIG. 68. Magneto-dielectric anisotropy effect plotted versus temperature for normal distribution with different axial ratios, (3-D case).

The effect of the average volume on the temperature variation of the magneto-dielectric anisotropy effect is presented in Fig. 69.

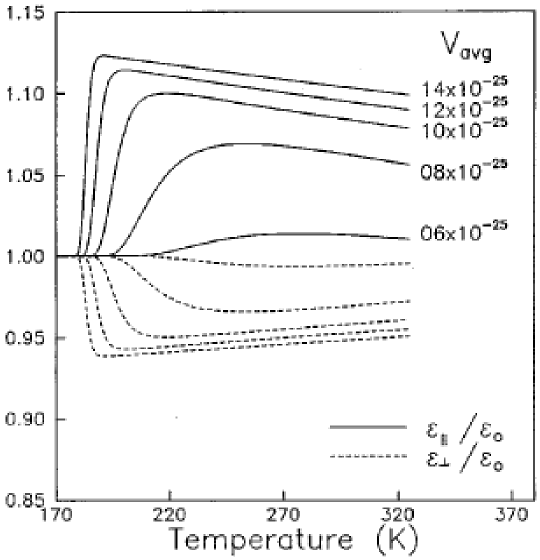

FIG. 69. Magneto-dielectric anisotropy effect plotted versus temperature for normal distribution with different average sizes, (3-D case).

The results in the figure show that the higher the average volume is the higher the effect is, and more importantly the lower the temperatures at which the onset of the dielectric anisotropy and the optimum conditions in the effect occur. Furthermore, the results also show that the rise to the maximum is steeper for higher average volumes. Noting that the Shliomis volume decreases with temperature around the slurry state of the sample and because a sample with a high average size will have larger particles than samples with lower average size, the unblocking of some particles occurs at lower temperatures for samples with high average size. Therefore, the onset in the dielectric anisotropy effect occurs at a lower temperature. Furthermore, a larger portion of the particles will be unblocked, at a given temperature, resulting in a steeper rise to the maximum for the samples with high average volumes and consequently the maximum is reached at a lower temperature.

The effect of the liquid carrier, i.e., initial viscosity and melting point of the carrier on the dielectric anisotropy is presented in Fig. 70. These results are obtained for a normal particle size distribution (V_{mean} = 10 × 10^{-25} m^3, σ = 1 × 10^{-25} m^3) and a measuring magnetic field (H = 39.8 kA/m). The liquid carriers used and their corresponding initial viscosities and melting points are listed in Table 3.

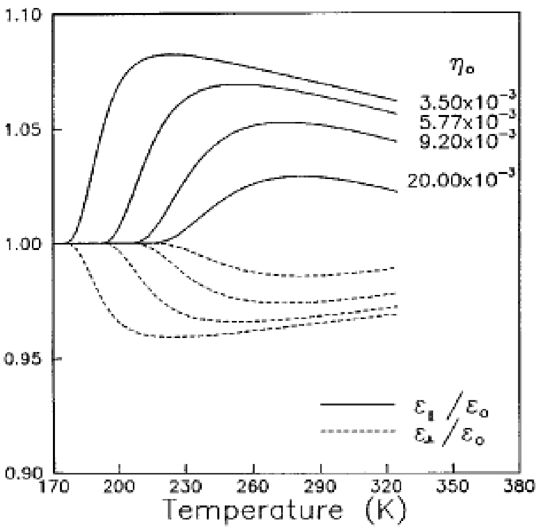

FIG. 70. Magneto-dielectric anisotropy effect plotted versus temperature for normal distribution and different liquid carriers, (3-D case).

The results in the figure show that the lower both the viscosity and the melting point of the carrier are, the lower both the temperatures at which the onset and the maximum in the dielectric anisotropy are. Furthermore, they also show that the lower η_o and T_o are the higher the dielectric anisotropy at a given temperature is.

Lowering the initial viscosity of the sample reduces the Brownian relaxation time at all temperatures and hence allows more particles to contribute to the dielectric anisotropy at lower temperatures. Furthermore, it also reduces the viscous torque thus making the magnetic torque capable of rotating the particles in the field direction. Hence, the temperature at which the onset of the dielectric anisotropy occurs is lowered. Decreasing the melting point of the carrier leads to a decrease in the melting point of magnetic fluid, consequently, the slurry state is reached in a less viscous sample before it is reached in a more viscous sample and as a result both the temperatures at which the onset and the maximum in the dielectric anisotropy are lowered by lowering the initial viscosity and melting point of the liquid carrier. For a low viscosity sample, a larger portion of the particles, in comparison to high viscosity sample, become unblocked at low temperature when the thermal agitation is not yet very effective in randomizing the particles, therefore, the dielectric anisotropy for low viscosity samples is larger than that for high viscosity samples. Although, this difference persists even at higher temperatures, but its value becomes less pronounced for higher temperatures.

Based on the orientation of the elongated particles in the magnetic field direction, that produces two different average projection lengths one is parallel, to the field and the other is normal to the field, the magneto-dielectric anisotropy was calculated. It is found that taken into consideration the competition between the N$e'el$ relaxation and the Brownian relaxation and the role of temperature in randomizing the already aligned particles, on the one hand, and of changing the viscosity on the other hand, is sufficient to produce all the basic features of the optical anisotropy that were observed experimentally. Therefore, it is concluded that the orientation of the particles and the chain formation in the fluid is the main cause of the magneto-dielectric anisotropy effect in magnetic fluids. Furthermore, it is shown that the magneto-dielectric anisotropy factor $g(H,\omega)$ is either 1.0 for 2-D sample or 2.0 for a 3-D sample. It is therefore suggested that dimensionality plays an important role in the magneto-dielectric anisotropy effect in magnetic fluids; and it is crucial to consider the dimensionality of the samples when comparing results obtained by different workers in the field.

References

[1]Rosensweig, R.E. "Ferrohydrodynamics", (Cambridge University press, Cambridge, 1985).

[2] Rosensweig, R.E., Ann. Rev. Fluid Mech. 19 (1987) 437.

[3] Blums, E., Cebers, A. and Maiorov, M.M. "Magnetic Fluids", (Walter de Gruyter, Berlin, 1997).

[4] Majorana, Q. C.R. Acad. Sci. Paris, 135 (1902) 159.

[5] Haas, W.L. and Adams, J.H., Appl. Phys. Lett. 27 (1975) 571.

[6] Popplewell, J., Davies, P., Bradbury A. and Chantrell, R.W., IEEE Trans. Magn. 22 (1986)1128.

[7] Hayes, C.F. and Hwang, S.R., J. Coll Int. Sci. 60 (1977) 159.

[8] Martinet, A., Rheol. Acta. 13 (1974) 260.

[9] Mairov, M.M., Magnetohydrodynamics, 3 (1977) 29.

[10]Neitzel, U. and Barner, K., Phys. Lett. A. 63 (1977) 474.

[11]Davies, H.W. and Llewellyn, J.P., J. Phys. D: Appl. Phys. 12 (1979) 311.

[12]Davies, H.W. and Llewellyn, J.P., J. Phys. D: Appl. Phys. 12 (1979) 1357.

[13]Bacri, J.C., Cabuil, V., Massart, R., Perzynski, P. and Salin, D., J. Magn. Magn. Mater. 65 (1987) 285.

[14]Scholten, P.C, IEEE Trans. Magn. 16, (1980) 221.

[15]Scholten, P.C., J. Magn. Magn. Mater. 39 (1983) 99.

[16] Hartmann, U. and Mende, H.H., J. Magn. Magn. Mater. 45 (1984)100.

[17]Hartmann, U. and Mende, H.H., Phys. Stat. Solidi, 82 (1984) 481.

[18]Yusuf, N.A., Abu-Safia, H. and Abu-Aljarayesh, I., J. Appl. Phys. 73 (1993) 6163.

[19]Abu-Safia, H., Abu-Aljarayesh, I., EI-Ghanem, H.M. and Yusuf, N.A., J. Magn. Magn. Mater. 103 (1992) 19.

[20]Yusuf, N.A., Abu-Safia, H., Abu-Aljarayesh, I. and Mahmood, S., J. Magn. Magn. Mater. 85 (1990) 85.

[21]Abu-Safia, H., Abu-Aljarayesh, I., Mahmood, S. and Yusuf, N.A., J. Magn. Magn. Mater. 87 (1990) 333.

[22]Mehta, R.V., Shah, H. S., Bahgat, J. B. and Bahgat, D.M., IEEE Trans. Magn. 16 (1980) 1324.

[23]Mehta, R.V. and Bhagat, D.M., IEEE Trans. Magn. 16 (1980) 258.

[24]Patel, R., Upadhyay, R.V. and Mehta, R.V. 300 (2006) e217.

[25]Scholten, P.C., Indian J. Eng. & Mater. Sci. 11 (2004) 323.

[26]De Gennes, P.G. and Pincus, P.A., Phys. Condens. Matter, 11 (1990) 189.

[27]Jones, G. A. and Niedoba, H., J. Magn. Magn. Mater. 73 (1988) 33.

[28]Yusuf, N.A., J. Phys. D: Appl. Phys. 22 (1989) 1916.

[29]Nair, S.S., Rajesh, S., Abraham, V.S., Anantharaman, M.R. and Nampoori, V.P.N., J. Magn. Magn. Mater, 305 (2006) 28.

[30]Pshenichnikova, A.F. and Fedorenkob, A.A., J. Magn. Magn. Mater. 292 (2005). 332,

[31]Fang, W.-X., He, Z.-H., Xu, X.-Q., Mao, Z.-Q. and Shen, H., EPL, 77 (2007) 68004.

[32]Elfimova, E., J. Magn. Magn. Mater. 300 (2006) 203.

[33]Taketomi, S., Ogawa, S., Miyajima, H. and Chikazumi, S., J. Magn. Soc. Jpn. 12 (1988) 263.

[34]Taketomi, S., Takahashi, H., Inaba, N., Miyajima, H. and Chikazumi, S., J. Phys. Soc. Jpn. 59 (1990) 2500.

[35]Taketomi, S., Ukita, M., Mizukumi, M., Miyajima, H. and Chikazumi, S., J. Phys. Soc. Jpn. 56 (1987) 3362.

[36]Shliomis, M.I., Sov. Phys. USP, 17 (1974) 153.

[37]Shliomis, M.I., Sov. Phys. JETP, 34 (1972) 1291.

[38]Shliomis, M.I. and Stepanov, V.I., J. Magn. Magn. Mater. 122 (1995) 176.

[39]Gladkov, S.O., Physica B, 160 (1989) 211.

[40]McTague, J.P., J. Chem. Phys. 51 (1969) 133.

[41]Yusuf, N.A., Manasrah, D.A., Abdallah, M.A., Abu-Safia, H. and Abu-Aljarayesh, I., J. Magn. Magn. Mater. 138 (1994) 173.

[42]Abu-Aljarayesh, I., Abdallah, M.A., Manasrah, D.A., Abu- Safia, H. and Yusuf, N.A., J. Magn. Magn. Mater. 138 (1994).

[43]Derriche, O., Jorat, L., Noyel, G., and Monin, J., J. Magn. Magn. Mater. 102 (1991)155.

[44]Colteu, A., J. Magn. Magn. Mater. 39 (1983) 88.

[45]Cotae, C., J. Magn. Magn. Mater. 39 (1983) 85

[46]Kopcansky, P., Cernak, J., Macko, P., Spisak, D. and Marton, K., J. Phys. D: Appl. Phys. 22 (1989) 1410.

[47]Kaplan, B.Z. and Jacobson, D.M., Nature (London), 259 (1976) 654.

[48]Mailfert, A.J. and Nahounou, B., IEEE Trans. Magn. 16 (1980) 254.

[49]Espurz, A., Alameda, J.M. and Espurz-Nieto, A., J. Phys. D: Appl. Phys. 22 (1989) 1174.

[50]Fannin, P.C., Scaife, B.K. and Charles, S.W., J. Magn. Magn. Mater. 122 (1993) 168.

[51]Chantrell, R.W., J. Magn. Magn. Mater. 45 (1984) 100.

[52]Chantrell, R.W., Popplewell, J. and Charles, S.W., IEEE Trans. Magn. 14 (1987) 975.

[53]Ayoub, N.Y., Bradburay, A., Chantrell, R.W. and Popplewell, J., J. Magn. Magn. Mater. 65 (1987) 185.

[54]Taketomi, S., Japan. J. Appl. Phys. 22 (1983) 1137.

[55]Davies, P., Popplewell, J. and Llewellyn, J.P., IEEE Trans. Magn. 22 (1986) 1131.

[56]Davies, H.W. and Llewellyn, J.P., J. Phys. D: Appl. Phys. 13 (1980) 3327.

[57]Kooij, E.S., Gâlcã, A.C. and Poelsema, B., J. Colloid. Inter. Sci. 304 (2006) 261.

[58]Rousan, A.A., Yusuf, N.A. and El-Ghanem, H.M., IEEE Trans. Magn. 24 (1988) 1653.

[59]Yusuf, N.A., Rousan, A.A. and El-Ghanem, H.M., J. Magn. Magn. Mater. 65 (1987) 282.

[60]Yusuf, N.A., Abu-Aljarayesh, I., Rousan, A.A. and El-Ghanem, H.M., IEEE Trans. Magn. 26 (1990) 2852.

[61]Rousan, A.A., El-Ghanem, H.M. and Yusuf, N.A., IEEE Trans. Magn. 25 (1989) 3121.

[62]Hui, P.M. and Stroud, D., Appl. Phys. lett. 50 (1987) 950.

[63]Maxwell-Garnet, J.C., Philos. Trans. R. Soc. London. 203 (1904) 385.

[64]Yusuf, N.A., Rousan, A.A. and El-Ghanem, H.M., J. Appl. Phys. 64 (1988) 2781.

[65]Yusuf, N.A., Japn. J. Appl. Phys. 28 (1989) 819.

[66]Llewellyn, J.P., J. Phys. D: Appl. Phys. 16 (1983) 95.

[67]Wiener, O., Abh. Sachs. Akad. Wiss. 32 (1912) 509.

[68]Yusuf, N.A., Shobaki, J., Abu-Safia, H. and Abu-Aljarayesh, I., J. Magn. Magn. Mater. 149 (1995) 373 .

[69]Yusuf, N.A., Ramadan, A. and Abu-Safia, H.A., J. Magn. Magn. Mater. 184 (1998) 375.

[70]Yusuf, N.A., Qasmieh, I. and Abu-Safia, H.A., J. Magn. Magn. Mater. 166 (1997) 374.

[71]Popplewell, J., Abu Aisheh, B. and Ayoub, N.Y., J. Appl. Phys. 64 (1988) 5852.

[72]Soffge, F. and Schmidbauer, E., J. Magn. Magn. Mater. 24 (1981) 54.

[73]Cullity, B.D., "Introduction to Magnetic Materials", (Addison-Wesley, New York, Reading, 1972).

[74]Maiorov, M.M., J. Magn. Magn. Mater. 252 (2002) 111.

[75]Socoliuc, V. and Bica, D., J. Magn. Magn. Matre, 289 (2005) 177.

[76]Morais, P.C., Gravina, P.P., Neto, K.S. and Lacava, B.M., Thin solid Films, 515 (2006) 226.

[77]Popescu, L.B., Socoliuc, V. and Bica, D., Rom. Journ. Phys. 51 (2006) 791.

[78]Yusuf, N. A., Arab. J. Sci. Eng. 15(2A) (1990) 219.

[79]Fredriq, E. and Houssier, C., "Electric Dichroism and Birefringence", (Oxford, The University press, 1973).

[80]Shobaki, J., Rawwagah, F., Abu-Aljarayesh, I. and Yusuf, N.A., J. Magn. Magn. Mater. 159 (1996) 367.

[81]Shobaki, J., Musameh, S., Rawwagah, F. and Yusuf, N.A., Phys. Rev. B, 54 (1996) 13063.